PAX8 orchestrates an angiogenic program through interaction with SOX17

Daniele Chaves-Moreira[1], Marilyn A. Mitchell[1], Cristina Arruza[1], Priyanka Rawat[1], Simone Sidoli[2,3], Robbin Nameki[4,5], Jessica Reddy[4,5], Rosario I. Corona[4,5], Sisi Ma[6], Boris Winterhoff[7], Gottfried E. Konecny[8], Benjamin A. Garcia[2], Donita C. Brady[9,10], Kate Lawrenson[4,11], Patrice J. Morin[1] and Ronny Drapkin[1*].

[1]Ovarian Cancer Research Center, Department of Obstetrics and Gynecology, University of Pennsylvania Perelman School of Medicine. Biomedical Research Building II/III, Suite 1224, Philadelphia, PA, USA.
[2]Epigenetics Institute, Department of Biochemistry and Biophysics, Smilow Center for Translational Research, University of Pennsylvania Perelman School of Medicine, Suite 9-124, Philadelphia, PA, USA.
[3]Current affiliation: Department of Biochemistry, Albert Einstein College of Medicine, Bronx, NY, USA.
[4]Women's Cancer Program at the Samuel Oschin Comprehensive Cancer Center, Cedars-Sinai Medical Center, Los Angeles, CA, USA.
[5]Division of Gynecologic Oncology, Department of Obstetrics and Gynecology, Cedars-Sinai Medical Center, Los Angeles, CA, USA.
[6]Institute for Health Informatics, University of Minnesota, MN, USA.
[7]Department of Obstetrics, Gynecology and Women's Health, Division of Gynecologic Oncology, University of Minnesota, Minneapolis, MN, USA.
[8]Department of Medicine, David Geffen School of Medicine, University of California Los Angeles, Los Angeles, CA. USA.
[9]Department of Cancer Biology, University of Pennsylvania Perelman School of Medicine. Biomedical Research Building II/III, Suite 612, Philadelphia, PA, USA.
[10]Abramson Family Cancer Research Institute, University of Pennsylvania Perelman School of Medicine. Biomedical Research Building II/III, Suite 612, Philadelphia, PA, USA.
[11]Center for Bioinformatics and Functional Genomics, Cedars-Sinai Medical Center, Los Angeles, CA, USA.

***Correspondence:** rdrapkin@pennmedicine.upenn.edu

Keywords: PAX8, SOX17, SERPINE1, Transcription factor, Gene regulation, Ovarian Cancer, Fallopian tube, Tumor angiogenesis.

ABSTRACT

Worldwide, the number of new ovarian cancer cases approaches 300,000 with more than 180,000 deaths every year. The low survival-rate reflects the limitations of current therapies and highlights the importance of identifying new therapeutic targets. Despite significant recent efforts to identify novel vulnerabilities in ovarian cancer, none have led to effective durable therapies with improvement in overall survival. PAX8, a lineage-transcription factor, whose expression is a major molecular feature of ovarian carcinomas, represents a novel therapeutic target. Herein, we have identified SOX17 as a *bona fide* PAX8-interacting partner and elucidated the impact of this interaction on the development of ovarian cancer. Importantly, we found that PAX8 and SOX17 regulate tumor angiogenesis *in vitro* and *in vivo*. The role of PAX8 and SOX17 in the regulation of angiogenesis reveals a novel function for these factors in regulating the tumor microenvironment and highlight this pathway as a viable therapeutic target.

INTRODUCTION

Epithelial ovarian carcinoma is the most lethal of all gynecologic malignancies, claiming an estimated 14,000 lives annually in the United States of America (1) with worldwide numbers approaching 180,000 deaths annually (2). The lack of effective screening tools result in the majority of cases being diagnosed at an advanced stage and thus translating into a 5-year survival rate of less than 30% (3). The absence of adequate screening is compounded by the propensity of this disease to acquire chemoresistance and relapse of disease in the majority of patients despite initial response to platinum-based chemotherapy and surgical cytoreduction. Although much progress in ovarian cancer disease knowledge has emerged, effective targeted therapies have yet to impact overall survival rates (4).

The knowledge of the pathogenesis of high-grade serous ovarian carcinoma (HGSOC), the most common subtype of this disease, has greatly advanced over the past decade. A number of studies support the fallopian tube secretory epithelial cells (FTSEC) as the site of origin of the majority of HGSOC (5-13). The development of female reproductive tract is governed by the PAX8 transcription factor (14), which is a member of the Paired-Box family of transcription factors that play essential roles during embryogenesis and tumorigenesis (15). In normal oviducts, PAX8 expression is restricted to the secretory cells while neighboring ciliated cells show no expression. The sustained expression of PAX8 in the adult FTSEC and in nearly all HGSOCs (16), previously led us to use the PAX8 promoter to develop a genetically engineered mouse model of HGSOC (17, 18). Knockdown of PAX8 in ovarian cancer cells leads to apoptosis (19-21) supporting a definitive role for PAX8 in ovarian cancer growth and progression. However, it remains unclear how PAX8 drives the development of the Mullerian reproductive tract or how it supports neoplastic growth.

Surprisingly, PAX8 knockdown following transcriptome analysis revealed a negligible impact on the FTSEC cell lines with very few transcripts significantly affected by PAX8 loss (21, 22). In contrast, the range of transcripts altered by PAX8 loss in cancer cell lines was considerably higher. Ontology

analysis of the alterations after PAX8 loss showed changes in proliferation, angiogenesis and adhesion pathways that are crucial for tumor progression (22). Chromatin immunoprecipitation-sequencing (ChIP-seq analysis) showed that the PAX8 cistrome is reprogrammed during the process of malignant transformation by the widespread redistribution of PAX8 binding sites in the genome of ovarian cancer cells. Moreover, a recent study showed that non-coding somatic mutations disrupt the PAX8 transcriptional program in ovarian cancer (23).

To further survey the roles of PAX8 in ovarian carcinomas, we purified the PAX8 protein complex from a panel of different fallopian tube secretory cells, and different ovarian carcinoma cells and identified its components. Our analyses reveal that PAX8 is part of a NuRD chromatin remodeling complex and associates with multiple factors including SOX17. We show that depletion of PAX8 or SOX17 impacts the expression of factors involved in angiogenesis and functionally disrupts capillary formation *in vitro* and in mouse models. Disruption in angiogenesis greatly decreased tumor burden, ascites formation and lead to improved survival. These findings support a role of PAX8 and SOX17 in the regulation of angiogenesis and highlight this pathway as a viable therapeutic target.

RESULTS

Biochemical purification of the PAX8 complex

To better understand the function of PAX8 in benign compared to malignant fallopian tube secretory cells, we developed a biochemical affinity-purification method (Figure 1A). First, we generated nuclear extracts as previously described (24) and purified the endogenous PAX8 protein complex from three ovarian carcinoma cell lines (OVCAR4, KURAMOCHI, and OVSAHO) and three immortalized fallopian tube secretory cell lines (FT194, FT246, and FT282) using anti-PAX8-specific antibodies. Immunoblotting following affinity chromatography demonstrated the specific enrichment of PAX8 in our system (Figure 1B). When the affinity-purified PAX8 complex was evaluated on size-exclusion chromatography it revealed a size of approximately 600 kDa (Figure 1C). Mass spectrometry analysis of the PAX8-containing fractions identified a number of putative PAX8-interacting proteins (Figure 1D and Table 1).

Remarkably, many of the putative PAX8-interacting proteins represent components of chromatin-remodeling complexes. For example, chromodomain-helicase-DNA-binding protein 4 (CHD4), Transcriptional repressor p66-alpha (GATAD2A), Metastasis-associated protein 2 (MTA2), histone deacetylases 1 (HDAC1) and Retinoblastoma binding protein 4 (RBBP4) are components of the nucleosome remodeling and deacetylase (NuRD) complex. The NuRD complex is responsible for transcriptional repression through histone deacetylation and nucleosome remodeling (25). Coincidently, NuRD complex core members, as the helicase CHD4, was also found to be an interactor and epigenetic coregulator of PAX3-FOXO1 in alveolar rhabdomyosarcoma (26).

To prioritize the putative PAX8-interacting partners for further study, we ranked the peptides by confident identification score (i.e. MaxQuant score), correlation with PAX8 expression in ovarian tumor tissues, and co-dependency in ovarian carcinoma cell lines. SOX17, a member of the Sry-related HMG box transcription factors family, exhibited the strongest correlation, co-dependency with PAX8 in ovarian cancer, and was identified among the top-ranked most abundant putative PAX8-interacting

partners (Table 1 and SI 1). We confirmed SOX17 as a *bona fide* PAX8-interacting partner by showing co-immunoprecipitation using agarose beads covalently bound to either a specific anti-PAX8 or anti-SOX17 antibody, compared to rabbit IgG control beads (Figure 1E), indicating that PAX8 and SOX17 physically interact. Consistent with this finding, we observed co-elution of PAX8 and SOX17 in the same large molecular size fractions (Figure 1F), indicating that they are part of the same complex. We did not observe monomeric PAX8 or SOX17 in lower molecular weight fractions.

PAX8 physically interacts with SOX17 in high-grade serous ovarian carcinoma

We next characterized the location and levels of expression of PAX8 and SOX17 in five normal human fallopian tube tissues compared to five different HGSOC cases by immunohistochemistry. As shown in Figure 2A, we observed the co-expression of PAX8 and SOX17 restricted to the FT secretory epithelial cells. We also observed the over-expression of both PAX8 and SOX17 in all HGSOC cases (Figure 2A). Interestingly, PAX8 and SOX17 gene expression levels are significantly higher in ovarian cancers and in benign fallopian tubes than normal ovaries (SI 2A-2B-2C).

Our immunohistochemical findings are supported by high-resolution immunofluorescence analyses showing the nuclear co-localization of PAX8 and SOX17 in three different immortalized fallopian tube secretory cell lines (FT194, FT246, and FT282) and three high-grade serous ovarian carcinoma cell lines (OVCAR4, KURAMOCHI, and OVSAHO) (Figure 2B). To confirm the PAX8-SOX17 physical interaction, we performed an *in situ* proximity ligation assay (PLA), which allows the identification of both stable and transient interactions at native protein levels. We confirmed increased interaction between PAX8 and SOX17 in all tested high-grade serous cells: OVCAR4, KURAMOCHI, and OVSAHO (Figure 2C and SI 2D). As expected for transcription factors, the observed protein-protein interactions were nuclei localized. Moreover, we further explored the PAX8-SOX17 interaction in five different HGSOC tissue samples and again we observed a stronger and higher number of PLA signals in the cancer samples than in the normal fallopian tube samples (Figure 2D), confirming that the PAX8-

SOX17 interaction may be important in the process of malignant transformation. Moreover, in the normal fallopian tube cases, the PLA signals (PAX8-SOX17 interaction) were restricted to the secretory cells, reinforcing the hypothesis that these cells are the site of origin for HGSOC.

PAX8 and SOX17 are transcription co-regulators

To assess whether SOX17 and PAX8 could mutually regulate each other, we used RNA interference to knockdown each gene individually. After PAX8 knockdown, SOX17 protein levels were significantly reduced, in all tested FTSEC and HGSOC cell lines, and actually became undetectable in some lines (Figure 3A-3B and SI 3). Conversely, SOX17 knockdown also led to a decrease in the PAX8 protein level, but the effects were much less pronounced. At the RNA level, PAX8 loss led to a significant decline of SOX17 expression in all cell lines studied (Figure 3C) and SOX17 knockdown similarly led to a decrease of PAX8 expression (Figure 3D). These data suggest that SOX17 and PAX8 can transcriptionally regulate each other's mRNA expression and that, in the absence of PAX8, SOX17 protein is rapidly depleted.

Since the PAX8-SOX17 complex appears to transcriptionally regulate the PAX8 and SOX17 promoters, we performed luciferase reporter assay to directly test the transcriptional effect of this complex on minimal promoters containing five times PAX8 binding sites (27). Consistent with the results described above, knockdown of either PAX8 or SOX17 demonstrated a significant decline of luciferase activity mediated by PAX8-binding sites (Figure 3E-3F).

PAX8 and SOX17 regulate a common set of genes

To determine which pathways are regulated by the PAX8-SOX17 complex, we first performed RNA-seq following depletion of each factor individually, and in combination (siDUAL). Control cells received a non-targeting siRNA control pool (siNT). The efficiency of the knockdowns was assessed both by the number of sequenced reads, and Western blot (SI 3). Unsupervised analysis of the

significantly altered transcripts after the loss of PAX8, SOX17, or both together is shown in Figure 4A and Table 2. PAX8 and SOX17 can both negatively and positively regulate gene expression. PAX8 target genes were significantly more likely to be regulated by SOX17 than expected by chance ($p < 0.00001$, Chi-squared test). Treatment with siRNAs to simultaneously deplete both factors largely phenocopied the maximal effect of either siPAX8 or siSOX17 (Figure 4A). We focused on the 380 genes that were commonly up-regulated (Figure 4B) under all three conditions. These genes were enriched in pathways associated with cell adhesion, blood vessel development, and angiogenesis (Figure 4C).

In order to further characterize the gene regulation coordinated by PAX8/SOX17, we performed targeted functional proteomic profiling using reverse-phase protein arrays (RPPA)s. Knockdown of PAX8, SOX17 or both resulted in significant changes across 142 proteins (Figure 4D and Table 3). Consistent with our observations made using RNA-seq, ontology analysis of the identified target genes showed that cell adhesion, and angiogenesis were among the pathways most significantly altered after PAX8 and/or SOX17 loss (SI 4C). When examining individual genes, we found that Serpin Family E Member 1 (SERPINE1), also called Plasminogen Activator Inhibitor 1 (PAI1), was the most highly elevated protein following knockdowns (Figure 4E). The protein data corroborate the RNA-seq analysis which also found SERPINE1 mRNA levels the most commonly up-regulated (SI 4A-4B). Interestingly, this gene has been implicated as an inhibitor of the tissue-type plasminogen activator and angiogenesis (28). Using immunoblotting and quantitative-PCR, we confirmed that PAX8 or SOX17 knockdown significantly increased the expression of SERPINE1 and all tested cells (Figure 4F-4G). Moreover, SERPINE1 presented a strong differential expression pattern between benign and malignant cells. All FTSEC lines exhibited higher levels of SERPINE1 compared to isogenic oncogene-transformed lines or ovarian cancer cell lines (SI 4D) and this expression was inversely correlated with the levels of PAX8/SOX17 (SI 4E). This suggests an important role for PAX8-SOX17-mediated SERPINE1 suppression in malignant transformation.

SERPINE1 participates in PAX8-SOX17-mediated angiogenesis

Using an angiogenesis antibody array, we further examined the levels of 35 different secreted angiogenesis mediators in a panel of human ovarian carcinoma cells (OVCAR3, OVCAR4, KURAMOCHI, and OVTOKO) and a panel of human fallopian tube secretory cells (FT33, FT194, FT246, and FT282). The FTSEC line-conditioned media exhibited a higher concentration of the angiogenesis inhibitors such as SERPINE1 and THBS1, while the ovarian cancer lines secreted more angiogenesis inducers such as VEGFA, CXCL8, and CXCL16 (Figure 5A and SI 5). We found that some angiogenic factors were regulated by PAX8 and SOX17. Indeed, VEGFA, CXCL8, and CXCL16 exhibited reduction after the knockdown of PAX8 or SOX17 in the cancer lines, while their secretion in the normal lines was not detected (Figure 5B). However, the most prominent effect observed in cancer cell lines was a large increase in SERPINE1 secretion following PAX8 knockdown. SERPINE1 is particularly interesting because its secretion levels were also elevated in FTSECs compared to ovarian cancer lines. Indeed, FTSEC-conditioned media presented an average of 20 ng/mL of SERPINE1, which was many times higher than the secretion from ovarian cancer lines, an average of 0.2 ng/mL (Figure 5C-5D). Corroborating our previous findings, the secretion of SERPINE1 was significantly increased in HGSOC conditioned media following PAX8 or SOX17 knockdown (Figure 5E-5F).

Roles of SERPINE1 and its regulators, PAX8 and SOX17, on ovarian tumor angiogenesis.

Using the human umbilical vein endothelial cells (HUVEC) tube-formation assay, we found that conditioned media from ovarian carcinoma cells induced the formation of blood vessels *in vitro*, although not to the same extent as recombinant VEGF. This effect was almost abolished in conditioned media from ovarian cancer lines with PAX8 or SOX17 knockdown (Figure 6A). However, no induction of HUVECs tube formation was observed with the FTSEC lines conditioned media, which exhibit a higher concentration of SERPINE1 (Figure 6A-6B). We further investigated the VEGFR2 pathway status and corroborated the inactivation of the downstream effectors PLCy1 and ERK1/2 in endothelial

cells exposed to HGSOC conditioned media after the loss of PAX8 or SOX17 when compared with the no-targeting control knockdown (SI 6).

To extend these findings to an *in vivo* system, we performed in nude mice the directed *in vivo* angiogenesis assay (DIVAA) (29, 30). The DIVAA assay uses semi-closed small silicone cylinders known as angioreactors. The cylinders can be filled with angiogenic or antiangiogenic compounds of interest. Following subcutaneous implantation in nude mice, host vascular endothelial cells will migrate into the angioreactors and proliferate to form new blood vessels, if the compound of interest is angiogenic. In the presence of VEGF, used as a positive control, a strong induction of angiogenesis was observed (Figure 6C-6D). No significant blood vessels were observed in the vehicle (PBS or Fresh Media) control or with SERPINE1. Cylinders containing HGSOC cell lines conditioned media revealed extensive angiogenesis. The presence of erythrocytes inside the newly developed blood vessels indicated that they were functional. In contrast, conditioned media from HGSOC cell lines with PAX8 or SOX17 knocked down showed a significant decrease in ovarian cancer-induced neovascularization. These results show that ovarian cancer cell lines have the capacity to induce angiogenesis *in vivo*, and that PAX8 and SOX17 participate in this process probably through SERPINE1 down-regulation.

Knockdown of PAX8 or SOX17 decreases tumor formation in an ovarian cancer xenograft model.

Because we observed significant and reproducible effects of PAX8/SOX17 on angiogenesis, we hypothesized that knockdown of these genes may reduce the capacity of malignant cells to develop tumors *in vivo*. We employed a doxycycline-inducible lentiviral shRNA system in order to express shRNAs against PAX8 or SOX17 to deplete PAX8 or SOX17 levels in 3 different cancer cell lines (OVCAR3, OVCAR4, and OVTOKO). Unfortunately, OVCAR3 and OVCAR4 cells appeared to be exquisitely sensitive to the loss of PAX8 and SOX17 and we were unable to identify clones with acceptable levels of down-regulation. However, some OVTOKO clones exhibited efficient PAX8 or

SOX17 knockdown and up-regulation of SERPINE1 after the induction with doxycycline (Figure 7A). OVTOKO-shRNA harboring cells were injected intraperitoneally into NSG mice and incubated for 72 hours before doxycycline was added to the diet. After two weeks, control mice exhibited a significant tumor burden (Figure 7B). Doxycycline treatment reduced the tumor burden further to an almost undetectable level with no signs of ascites (Figure 7C-7D-7E), reinforcing our hypothesis that PAX8/SOX17 are modulating tumor angiogenesis by suppressing anti-angiogenesis factors as SERPINE1 and THBS1 (SI 7). These data show that inhibition of PAX8/SOX17 profoundly impairs the growth of ovarian carcinoma cells in mice, part of these effects likely due to suppression of tumor angiogenesis.

DISCUSSION

Many studies have implicated PAX8 as an important transcription factor in ovarian cancer. However, its mechanism of action in this regard remains unclear. Here, using a combination of biochemistry, *in vitro* models, and animal studies we make two important observations about how PAX8 governs tumor development. We show that PAX8 interacts with another developmental transcription factor, SOX17. PAX8 regulates expression of SOX17 and together they mediate a transcriptional program that drives angiogenesis in the malignant setting. Depletion of these proteins greatly attenuates angiogenesis in multiple systems.

Previous studies have shown that benign and malignant cells are distinguished by marked remodeling of the PAX8 cistrome and this implies that PAX8 may acquire new targets or functions in the malignant state (22). To investigate if the PAX8 re-distribution in cancer cells was due to changes in the PAX8 network, and to further clarify its roles in ovarian cancer, and possibly identify novel therapeutic opportunities, we first sought to identify its interacting partners in benign and malignant cells. Interestingly, its crucial role in transcriptional regulation was highlighted by our finding that multiple chromatin remodeling proteins interact with PAX8. Mechanisms of gene regulation by PAX8 are clearly complex as we found that, following PAX8 knockdown, a vast number of genes were up-regulated or down-regulated in these cells. A large number of the nucleosome remodeling molecules identified here are subunits of the NuRD complex, such as CHD4, MTA2, GATAD2A, GATAD2B, HDAC1, and RBBP4 suggesting that PAX8 participate in this chromatin-remodeling complex. Reinforcing these findings, a recent drug screen showed that PAX8 levels were strongly decreased by inhibitors of histone deacetylase (HDAC1) (31). Among the interacting partners identified, SOX17 was one of the mostly highly enriched in our mass spectrometry data. In addition, it exhibited a strong correlation and co-dependency with PAX8 in ovarian cancer using TCGA gene expression data. SOX17 is a transcription factor and member of the SOXF family, which has an HMG, β-catenin binding and transactivation domains (32). SOX17 biological function is always dependent on a dimerization partner (33) that is

dynamic and specific to the cell context. SOX17-interacting partners can engage differentially in the genome, regulating different sets of genes (34). Therefore, we hypothesized that the PAX8-SOX17 transcriptional activity may be crucial in ovarian tumorigenesis. We found that both PAX8 and SOX17 exhibit expression in the nuclei of both benign and malignant secretory cells, where they physically and functionally interact. Our findings are in agreement with the current literature showing that PAX and SOX members can engage in transcriptional regulation. Indeed, PAX3 and SOX10 can physically interact and synergistically regulate MITF and c-RET enhancers (35). The PAX3-SOX10 interaction is important for melanoma cells, where these factors regulate cell motility, apoptosis, and proliferation (36). Additionally, PAX6 and SOX2 are also interacting partners in early neural differentiation and are necessary for neural progenitor cell pluripotency (37). Furthermore, PAX6 and SOX2 act as an oncogene and can induce cancer cell stemness (38).

We found that PAX8 and SOX17 can mutually regulate each other at the transcriptional level. At the protein level, PAX8 knockdown led to an almost complete disappearance of SOX17, and SOX17 knockdown led to a significant decrease in PAX8 levels. These results are reinforced by our recent findings showing that PAX8 and SOX17 were found to be master transcription factors that occupy regulatory elements related to their own encoding genes in ovarian cancer (39). Globally, PAX8 and SOX17 genomic binding sites co-localize within candidate active enhancers in HGSOC cell lines. In addition, PAX8 binds with high intensity near SOX17 gene locus, which confirms the co-regulation observed in SOX17 transcript and protein levels (39). Here, using transcriptomic and proteomic analyses we showed that PAX8 and SOX17 commonly regulate a family of genes associated with blood vessel formation, suggesting a cooperative role in orchestrating an important pro-angiogenic transcriptional program in ovarian cancer. In this setting, it is interesting to note that murine Sox17 can promote tumor angiogenesis and is regulated by the Notch pathway, known to contribute to angiogenesis (40-43).

Angiogenesis is a dynamic process rigorously regulated during embryogenesis, tissue regeneration, and ovulation. However, angiogenesis can also abnormally occur during malignant transformation (44, 45). Most of the angiogenesis mediators are secreted cytokines, but matrix metalloproteinases and integrins also participate in new blood vessel development (46). The most commonly secreted mediator in tumor angiogenesis is Vascular Endothelial Growth Factor (VEGF). VEGF acts through its receptor (VEGFR2) and downstream effectors such as PLCy1 and ERK1/2. Furthermore, VEGF signaling pathway abrogation has emerged as an attractive strategy of new targeted anti-cancer therapy (47). Indeed, we found that PAX8 and SOX17 loss triggered a reduction in angiogenesis both *in vitro* and *in vivo* model. We also observed a drastic decrease in tumor xenograft growth following PAX8/SOX17 knockdown, and while we cannot rule out the roles of other cell intrinsic processes, the decrease in angiogenesis is likely an important factor. It has been reported that patients with high levels of VEGF have the worst prognostic and lower survival rates. Moreover, ovarian cancer cells express on their surface VEGF receptors that contribute to angiogenesis and malignant progression (48). The VEGF pathway is also responsible for the formation of ascites in patients with ovarian tumors due to the elevated vascular permeability within peritoneal lining in the abdominal cavity (49). Consistent with this fact, we found a significant decrease in ascites formation following knockdown of PAX8 and SOX17.

In trying to better understand the mechanisms of angiogenesis orchestrated by PAX8 and SOX17, we examined individual genes and identified those that were most affected by the knockdowns. We found SERPINE1 to be the most highly commonly up-regulated gene both at the transcript level (using RNA-seq) and protein level (through RPPA). SERPINE1 is a serine proteinase inhibitor, belonging to the Serpin family, which is an important endothelial plasminogen activator inhibitor and urokinase inhibitor (50). Important roles in coagulation, extracellular matrix remodeling, and angiogenesis have been reported for SERPINE1. The anti-angiogenic effects of SERPINE1 seem to be mediated by binding to vitronectin and blocking αvβ3 and uPAR binding sites (51). Therefore,

binding of secreted SERPINE1 to vitronectin blocks cell adhesion, migration, and inhibits angiogenesis (52). Moreover, vitronectin and integrin-αvβ3 strongly intensify VEGFR2 activation by VEGF (53). SERPINE1 acts as an angiogenesis inhibitor by blocking the vitronectin-integrin-VEGFR2 axis and simultaneous abrogation of the VEGF-signaling pathway. Our set of experiments involving endothelial cell tube formation *in vitro* and the migration of endothelial cells into subcutaneous implants *in vivo* suggest that SERPINE1 is an essential inhibitor of tumor angiogenesis and is under PAX8-SOX17 regulation. Based on these experiments, we hypothesize that suppressing SERPINE1 through malignant transformation, triggers VEGFR2 activation *in vivo* and contributes to tumor angiogenesis (SI 7).

Our results may also help explain some of the developmental defects described in the *Pax8* knockout mouse (14). *Pax8*$^{-/-}$ mice are infertile because they lack a functional uterus revealing only remnants of myometrial tissue. In addition, the vaginal opening is absent. Folliculogenesis, ovarian hormone production, and transcription of pituitary hormones are in a normal range. Thus, infertility in *Pax8*$^{-/-}$ mice seems to be due to a defect in development of the reproductive tract rather than to hormonal imbalance, pointing to a direct morphogenic role for Pax8 in uterine development. Our observation that Pax8 and Sox17 orchestrate an angiogenic program may help explain the atresia of the reproductive tract seen in the *Pax8*$^{-/-}$ mice. The absence of Pax8 in the developing reproductive tract is likely accompanied by low Sox17 and high Serpine1. These conditions would effectively shut down blood vessel development and prevent the development of the organ. This is reminiscent of the severe embryopathy seen with thalidomide in the early 1960s (54). Thalidomide was marketed as an anti-emetic which was later shown to have anti-angiogenic properties that cause severe birth defects, including phocomelia (limb defects), genital, and internal organ absence or malformation.

In summary, we have shown for the first time that PAX8 physically interacts with SOX17 in FTSEC and HGSOC leading to changes in multiple transcriptional programs, including modulation of genes mediating tumor angiogenesis. Further analyses of the genes regulated by PAX8/SOX17

identified SERPINE1 as an anti-angiogenic factor that is suppressed by PAX8-SOX17 in cancer cells. Knockdown of PAX8/SOX17 in this setting results in a decrease of blood vessel formation. Using cell-based and animal models, we then functionally demonstrate that PAX8/SOX17 can regulate angiogenesis during tumor development. Inhibition of tumor angiogenesis, perhaps through PAX8/SOX17 pathway inhibition, has potential value as part of an anti-angiogenic approach to the treatment of ovarian cancer (40, 55).

METHODS

Cells and Tissues

Human immortalized fallopian tube secretory cells (FT33, FT194, FT246, and FT282) were maintained in standard conditions as previously described (56) and grown in DMEM/F12 containing 2% Ultroser-G serum substitute. Human ovarian cancer cells were acquired from different sources. OVCAR3 was obtained from ATCC and maintained as recommended. OVCAR4 was acquired from William C. Hahn's lab-CCLE (Dana-Farber Cancer Institute) and grown in RPMI 1640 containing 10% fetal bovine serum. KURAMOCHI, OVSAHO, and OVTOKO were obtained from JCRB and maintained as recommended. The human umbilical vein endothelial cells (HUVEC) were acquired from Sigma-Aldrich and maintained according to manufacturer instructions. All cell lines were sent to the Wistar Institute Genomic Core Facility for authentication using short tandem repeat profiling and for detection of *Corynebacterium bovis* infection. In addition, all cell lines were also tested for *Mycoplasma* sp. at the University of Pennsylvania Cell Center.

Following approval by the Hospital of Pennsylvania Institutional Review Board, we obtained human fallopian tube and human high-grade serous ovarian carcinoma formalin-fixed and paraffin-embedded sections from the Department of Pathology at HUP to evaluate the expression of PAX8 and SOX17.

Purification of endogenous PAX8

Benign and malignant cells were grown in 15-cm plates until 90% confluence, washed twice with PBS, trypsinized, neutralized and collected. Nuclear fractionation was prepared as previously published (24). Harvested cells were resuspended in hypotonic buffer [20 mM HEPES, pH 7.5, 10 mM KCl, 1 mM EDTA, 1 mM EGTA, 1.5 mM $MgCl_2$, 2 mM dithiothreitol, protease inhibitors (Sigma-Aldrich: P8340), and phosphatase inhibitors (Sigma-Aldrich: P5726)] and incubated for 30 minutes. Samples were then disrupted through a 22G needle and centrifuged at 10,000 x *g* for 10 minutes at 4°C. Nuclei-enriched

fraction was sonicated with complete RIPA buffer (Cell Signaling: 9806S) containing protease inhibitors (Sigma-Aldrich: P8340), and phosphatase inhibitors (Sigma-Aldrich: P5726), and spun down for 10 minutes at 10,000 x g at 4°C. The supernatant (500 μg of nuclear extract) was incubated for 16 hours at 4°C with 105 μg of PAX8-specific antibody (Proteintech: 10336-1-AP) coupled to 1 ml of Protein A agarose resin (Thermo-Fisher: 44893) or with 105 μg of normal rabbit IgG (Proteintech: 30000-0-A) coupled to 1 mL of Protein A agarose resin, as negative control. The columns were washed three times with 10 mL of 0.1 M phosphate and 0.15 M NaCl, pH 7.2 and eluted with 0.5 M NaCl and 0.1 M glycine, pH 2.8. Fractions had their pH equilibrated with 1M Tris, pH 9.5, separated by gel electrophoresis, Coomassie blue-stained and lanes were sent for mass spectrometry analysis.

The affinity column eluates containing PAX8 were also loaded in 100 ml of Sephacryl S-300 column (Sigma-Aldrich: S300HR-100ML) equilibrated with 50mM Tris, pH 7.5, 100 mM KCL, 0.5 M NaCl, 1% NP-40 and 1% glycerol. We collected one hundred and fifty 500 μL fractions and protein peaks were separated by gel electrophoresis, silver-stained (Thermo-Fisher: 24600), checked by WBs for the presence of PAX8, and positive-samples were also sent for mass spectrometry analysis.

PAX8 interacting-partners identification

Coomassie blue-stained lanes containing PAX8 were analyzed by nanoLC-MS/MS setup as previously described (57). In summary, HPLC gradient was set between 0-30% of solvent A = 0.1% formic acid and solvent B = 95% acetonitrile, 0.1% formic acid for one hour followed by five minutes of 30% to 85% of solvent B and ten minutes of isocratic 85% solvent B. Flow rate of nLC was set to 300 nL/min and coupled to Orbitrap Fusion Tribrid mass spectrometer (Thermo Fisher, USA) with 2.5 kV spray voltage and 275 °C of capillary temperature. Full mass spectrometry was performed using a resolution of 120,000 and 27 of HCD.

DDA files were analyzed with MaxQuant (58) using a SwissProt human database. iBAQ quantification was used for enrichment analysis and data were log2 transformed and normalized by subtracting the average of all valid values for each sample. Statistics analysis was obtained applying a two-tails heteroscedastic t-test.

Co-immunoprecipitation.

500 µg of nuclear lysates were incubated with 25 µg of a specific PAX8-antibody (Novus: NBP1-32440), 25 µg of a specific SOX17-antibody (Abcam: ab224637), or 25 µg of a normal rabbit IgG (Cell Signaling: 2729S) covalently-coupled to activated agarose beads (Thermo-Fisher: 26148) as manufacturer's recommended protocol.

Conditioned medium

Secretory cells and carcinoma cells were growth in 60 mm dish at 37 ºC and 5% CO_2. Conditioned media were retrieved by spinning down at 2,000 x g for 5 minutes at 4 ºC then supernatants were passed through 0.22 µm filter (Millipore: SLGP033RS).

Immunohistochemistry

Fallopian tube and high-grade ovarian carcinoma sections were processed as previously reported (59). The immunohistochemical staining were performed using a dilution of 1:500 of anti-PAX8 antibody (Novus: NBP1-32440) or a dilution of 1:500 of anti-SOX17 antibody (Novus: NBP1-47996). Slides were scanned with Aperio CS2.

Immunofluorescence

Ten thousand FTSEC and HGSOC cells were seeded on imaging plates (Eppendorf: 0030741030) and allowed to grow for 24 hours. Following cells were washed twice in PBS and fixation

was performed for 15 minutes on Paraformaldehyde 4% (Thermo-Fisher: AAJ19943K2) at room temperature. After the incubation period, cells were washed twice in PBS and permeabilized with Triton X-100 0.25% (Boston BioProducts: P-924) for 15 minutes. Aldehydes residues were quenched with Glycine 100 mM (Sigma-Aldrich: 50046-50G) for 15 minutes. The unspecific sites were blocked with a solution of 1% bovine serum albumin, and 0.1% Tween 20 in PBS for 30 minutes. Samples were incubated for 16 hours with a dilution of 1:500 of anti-PAX8 (Novus: NBP1-32440) or a dilution of 1:500 of anti-SOX17 (Novus: NBP1-47996) at 4 ºC. Cells were then washed three times of 5 minutes each with a solution of 1% bovine serum albumin, and 0.1% Tween 20 in PBS followed by incubation for one hour with anti-mouse-AlexaFluor488 or anti-rabbit-AlexaFluor594. Cells were washed three time in PBS, mounted in Fluoromount-G with DAPI, and Images were acquired at 60X magnification employing a Nikon Eclipse Ti inverted microscope.

in situ Protein-protein interaction analysis

Prior to the protein-protein interaction staining by *in situ* proximity ligation assay (PLA), tissue sections and cell lines were processed as described in the IHC and IF sections. PLA signals were determined employing Duolink Probes Anti-Mouse MINUS (Sigma-Aldrich: DUO92004) and Anti-Rabbit PLUS (Sigma-Aldrich: DUO92002) as manufacturer's recommended protocol following overnight incubation with anti-PAX8 mouse antibody 1:250 (Novus: NBP2-29903) and anti-SOX17 rabbit antibody 1:250 (Cell Signaling: 81778S) at 4 ºC. Red fluorescent signals was obtained using detection reagent red (Sigma-Aldrich: DUO92008) and chromogen signals was acquired using detection reagent brightfield (Sigma-Aldrich: DUO92012).

siRNA knockdown

Fallopian tube secretory and ovarian carcinoma cells knockdowns were performed by reverse transfection with a mixture containing of 30 nM of ON-TARGETplus Human PAX8 siRNA

(Dharmacon:L-003778-00-0005), ON-TARGETplus Human SOX17 siRNA (Dharmacon: L-013028-01-0005) or non-targeting siRNA as negative control (Dharmacon: D-001810-10-05), 3 x 10^5 cells, 10 µl of Lipofectamine RNAiMax (Thermo-Fisher: 13778075), and Opti-MEM reduced serum medium (Gibco: 31985088) as recommended by the manufacturer's protocol.

Western blot analysis

Samples were incubated with RIPA buffer (Cell Signaling: 9806S) for 30 minutes at 4°C followed by centrifugation at 10,000 x g for 5 minutes. Supernatants' protein concentration was estimated by BCA method (Thermo-Fisher: 23227). Thirty micrograms of each sample were mix with sample buffer loaded and separated using Mini-PROTEAN TGX 4-15% polyacrylamide gels (BioRad: 4561083) and Tris/Glycine/SDS buffer (BioRad: 1610732). TURBO transfer system (BioRad: 1704156) was employed to move separated samples from gels to PVDF membranes. Primary antibodies: anti-PAX8 (Novus: NBP1-32440), anti-SOX17 (Abcam: ab224637) or anti-GAPDH (Cell Signaling: 5174) were diluted 1:1000 in 5% nonfat milk in TBS containing 0.1% Tween 20 and incubated with the membranes overnight at 4°C. After the period of incubation, membranes were washed three times with TBS containing 0.1% Tween 20 then incubated with anti-Rabbit IgG-HRP conjugated (Cell Signaling: 7074). Images were acquired by chemiluminescence using Clarity ECL (BioRad: 1705062).

Real-time PCR

Samples total RNA was purified using the RNeasy Plus Mini Kit (Qiagen: 74134), quantified and used as a template for the synthesis of single-stranded cDNA employing the High Capacity cDNA Reverse Transcription Kit (Thermo-Fisher: 4374966). To access the gene expression changes we employed the TaqMan Assay (Thermo-Fisher: 4331182) using 100 ng of cDNA per 20 µL of final reaction with TaqMan Fast Advanced Master Mix (Thermo-Fisher: 4444557) as recommended by manufacturer's protocol.

RNA-seq

Transcriptome analysis of OVCAR4 cells after PAX8, SOX17 or both knockdown simultaneously was performed as previously described (39, 60). In summary, ovarian carcinoma cells had their RNA chemically purified using the Nucleospin RNA Plus kit (Macherey-Nagel: 740984.50) as recommended by the manufacturer's protocol. Poly-A non-stranded library were prepared using the newly extracted RNA and forty million reads were sequenced by BGI platform. Bioinformatic analyses were executed employing the R package DESeq2 (version 1.24.0). Significant changes were designated as log2 fold change ≥ 1 and adjusted p-value ≤ 0.01. Metascape tool was employed to identify the differentially enriched pathways.

Reverse-phase protein array

Arrays were performed at the Department of Bioinformatics and Computational Biology in MD Anderson Cancer Center as previously described (61, 62). The platforms contains over 300 antibodies exclusively validated with a Pearson coefficient > 0.7 of correlation between RPPA and WB were employed in the proteomic analysis (63). Spots intensities were generated by colorimetric reaction employing the Dako Cytomation-Catalyzed System.

Luciferase reporter assay

Briefly, half-million cells were co-transfected with 1 µg of PAX8-(Firefly) Luciferase reporter vector (27), 0.5 µg of CMV-(Renilla) Luciferase control vector (Promega: E2261) and 30 nM of PAX8, SOX17 or Non-targeting siRNA, using Lipofectamine 2000 (Thermo-Fisher: 11668027) as recommended by manufacturer's protocol. Plates containing the different transfected cells were incubated for 24 hours at 37°C before the luciferase activity was measured using the Dual-Glo luciferase detection kit (Promega: E2920).

Array and ELISA

Angiogenesis secreted mediators were identified from fallopian tube secretory cells and ovarian carcinoma cells conditioned media employing the Human Angiogenesis Antibody Array (R&D systems: ARY007). ELISA was employed for the precise quantification of VEGF (R&D systems: DVE00) and SERPINE1 (R&D systems: DSE100) also from cells conditioned media as recommended by the manufacturer's protocol. Fresh DMEM/F12 or RMPI media were tested and considered as the negative control.

In vitro angiogenesis assay

Twenty thousand HUVEC cells were seeded in reduced growth factor basement membrane extract (BME)-coated 96-well plate (R&D systems: 3470-096-K). Endothelial cells were exposed to 100 µl of the different benign or malignant cells conditioned media, 10 ng/ml VEGF (R&D systems: 293-VE-010) or 10 µg/ml SERPINE1 (R&D systems: 1786-PI-010) for 6 h at 37 °C. HUVEC cells were labeled with 2 µM Calcein AM as recommended by the manufacturer's protocol to facilitate the image acquisition using a Nikon Eclipse Ti inverted microscope. The number of complete endothelial loops per field were counted and compared.

In vivo angiogenesis assay

Following IACUC review and approval (Protocol #806687), *in vivo* angiogenic responses were analyzed by directed *in vivo* angiogenesis assay (DIVAA) (R&D systems: 3450-048-K) as recommended by the manufacturer's protocol. Briefly, six-week female nude mice (JAX: 002019) were kept in aseptic condition under the Stem Cell and Xenograft Core barrier at the University of Pennsylvania. Mice cohorts were anesthetized with 2% isoflurane prior the subcutaneously implantation of angioreactors i.e. one-centimeter flexible silicone cylinder. Dorsal-lateral incisions were made on each nude mouse, where angioreactors filled with FTSEC or HGSOC conditioned media, 10

ng/ml VEGF (R&D systems: 293-VE-010) or 10 µg/ml SERPINE1 (R&D systems: 1786-PI-010) were subcutaneously inserted under the skin and then sutured to cover the incisions. Angioreactors were retrieved after 14 days of incubation for careful collection of the mouse endothelial cells that were attracted and invaded the cylinders. Neovascularization was quantified by staining the endothelial cells with FITC-lectin and measuring the intensity of fluorescence within a Thermo-Fisher Fluoroskan Ascent FL fluorimeter at 485nm.

Doxycycline inducible knockdown

We employed Dharmacon SMARTvector inducible lentiviral shRNA that utilize the Tet-On 3G bipartite induction system and TurboGFP as a fluorescent reporter. This tightly regulated system consists of an inducible RNA polymerase II promoter, Phosphoglycerate kinase (PGK), which has been optimized for both minimal basal expression and potent activation upon induction by doxycycline on the TRE3G. Together, the Tet-On 3G protein and TRE3G promoter permit tight regulation of the shRNA expression, including potent induction, even at the low doxycycline doses that are required for *in vivo* xenograft studies. The selected shPAX8 (Dharmacon: V3IHSPGG-8017023), shSOX17 (Dharmacon: V3IHSPGG-6371478) and Non-Targeting Control (Dharmacon: VSC6580) high-titer lentivirus were used to transduce OVCAR3, OVCAR4 and OVTOKO cells as recommended by the manufacturer's protocol.

Generation of Luciferase-expressing cells

Ovarian cancer cell lines (5 x 10^4 cells per 24 well) in complete media containing 8 µg/mL Polybrene (Millipore-Sigma: TR-1003-G) were transduced with high-titer Luc-mCherry lentivirus (64). Lentivirus was produced with 3rd Generation Packaging System Mix (Abcam: LV053) in 293T cells transfected with Lipofectamine 3000 Reagent (Thermo-Fisher: L3000008) in OPTI-MEM medium

(Gibco: 31985-062). In order to produce high-titer particles, 293T transfected cells conditioned media were condensed with the Lenti-X Concentrator (Clontech: 631231) at 4°C for 24 hours.

Mice xenograft

Following IACUC review and approval (Protocol #806825), one million OVTOKO harboring shRNA-luciferase-positive cells were inoculated intraperitoneally into five-six weeks old female immunodeficient NSG mice (JAX: 005557). All NSG mice cohorts were aseptically housed under the Stem Cell and Xenograft Core barrier. After 72 hours post-injections, feeding supplemented with 1g/kg of doxycycline (Teklad: TD.06294) was made continuously available for the mice. Tumor progression was examined by bioluminescence imaging using the Lumina IVIS system and 150 mg/kg of Luciferin (Gold Biotechnology, 115144-35-9) in PBS. Animals were sacrificed when they reached IACUC pre-determined endpoints for ascites and tumor collection.

Statistical analysis

Representative graphics are displayed as mean and standard derivation of experiments replicates. Significant changes $P < 0.05$ between controls and knockdowns were acquired applying Student's test (GraphPad Prims 8).

ACKNOWLEDGMENTS

We recognize the Drapkin laboratory members for their helpful consideration and support in especially Kai Doberstein. We also acknowledge Cynthia Lopez-Haber for her technical insights, Gregory Dressler for sharing the PAX8-Luciferase reporter vector, and Andrew Kung for donating the FUW-Luc-mCherry vector. In addition, we are very grateful for the Stem Cell & Xenograft Core, the Quantitative Proteomics Resource Core, and the MD Anderson RPPA Core (NCI P30 CA16672) for technical assistance and resource access. We are also very appreciative of Tony Secreto and Lauren Schwartz support and expertise.

This work was supported by an NIH SPORE in ovarian cancer P50 CA228991 (R.D.), the Dr. Miriam and Sheldon G. Adelson Medical Research Foundation (R.D.), the Honorable Tina Brozman Foundation for Ovarian Cancer Research (R.D.), the Basser Center for BRCA (R.D.), the Claneil Foundation (R.D.), an NIH P01CA196539 (B.A.G), the Ann and Sol Schreiber Mentored Investigator Award (545754) from the Ovarian Cancer Research Alliance (D. C-M), and the Liz Tilberis Early Career Award (599175), also from the Ovarian Cancer Research Alliance (K.L.).

FIGURES

Figure 1: Three-step proteomic approach identifies putative PAX8-interacting partners. (a) Schematic of the workflow for the PAX8-interacting partner's identification. (b) Representative examples of endogenous PAX8 immunoprecipitation silver-stained gel and immunoblot from fallopian tube secretory cells (FT) and ovarian carcinoma cells (OV). IMR90 cells, which are PAX8 negative, were used as negative control (C). (c) Immunoblot of size-exclusion fractions showing the presence of PAX8 at 600 kDa size range. PAX8 immunoprecipitates and gel-filtration fractions were sent for mass spectrometry analysis. (d) Volcano plot of identified putative PAX8-interacting partners. (e) Confirmation of PAX8 and SOX17 interaction by co-immunoprecipitation experiments from FTSEC and HGSOC cell lines. (f) PAX8 and SOX17 immunoblots of size exclusion fractions demonstrate co-elution at 600 kDa size range fractions.

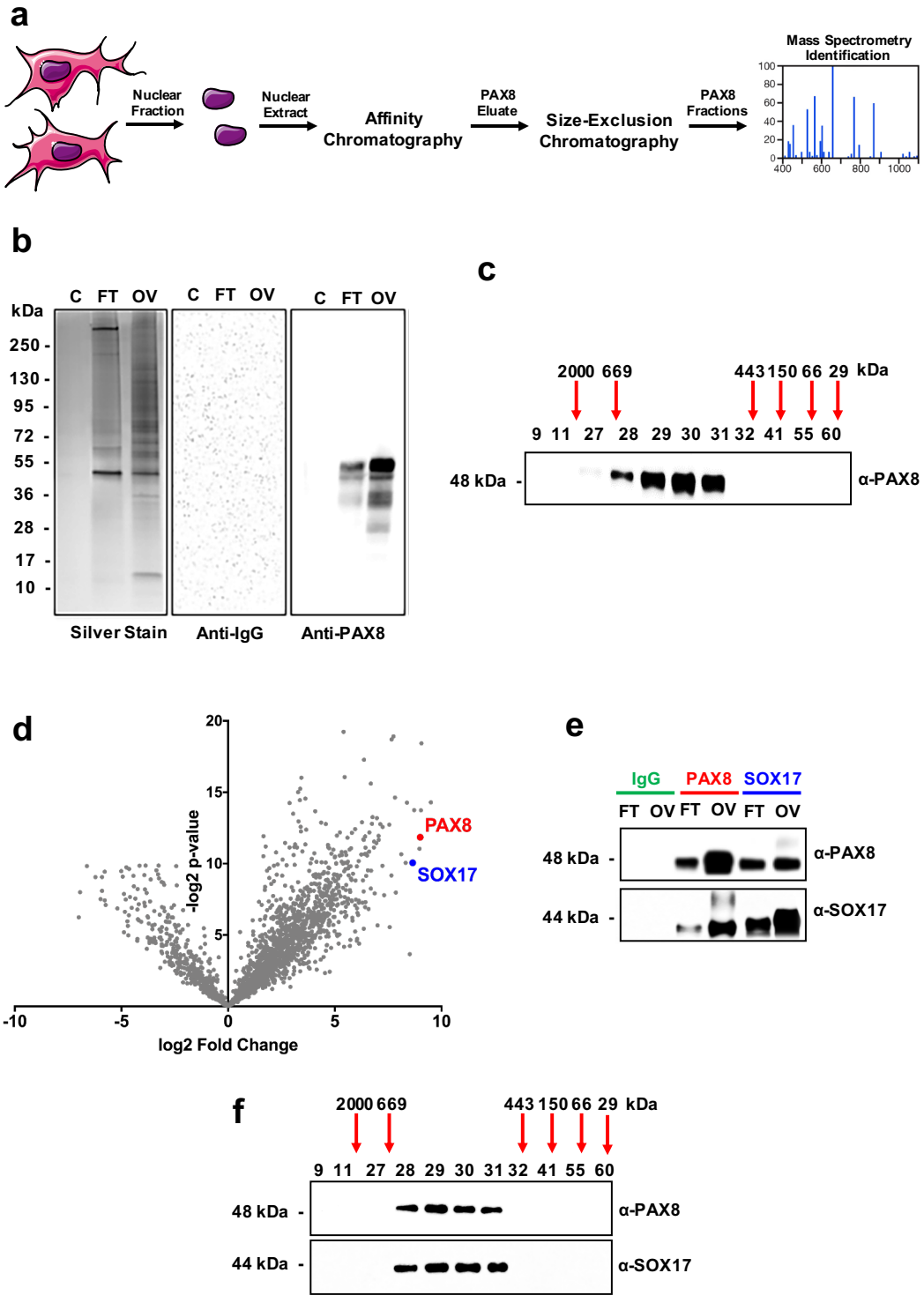

Figure 2: PAX8 physically interacts with SOX17 in the fallopian tubes and in ovarian cancer. (a) Immunohistochemistry showing nuclear co-expression of PAX8 and SOX17 in FTSEC and HGSOC cells. 5 normal samples and 5 ovarian cancer patients were analyzed and one representative case of each is shown. (b) Immunofluorescence showing co-localization of PAX8 and SOX17 in benign cells (FT194, FT246, and FT282) and in malignant cells (OVCAR4, KURAMOCHI, and OVSAHO). (c) Proximity ligation assay signals in secretory cells (FT194, FT246, and FT282) and in carcinoma cells (OVCAR4, KURAMOCHI, and OVSAHO) are shown in red. The nuclei are stained with DAPI (blue). The nuclei were acquired in one z-plane with 60X magnification. (d) *In situ* proximity ligation assay signals in normal fallopian tube sections and high-grade serous ovarian cancer samples shown in brown and the nuclei in orange. The nuclei were acquired in one z-plane with 40x magnification. *Number of PLA signals (PAX8-SOX17 interactions) was determined by counting 100 nuclei per sample (Supplemental information 2).

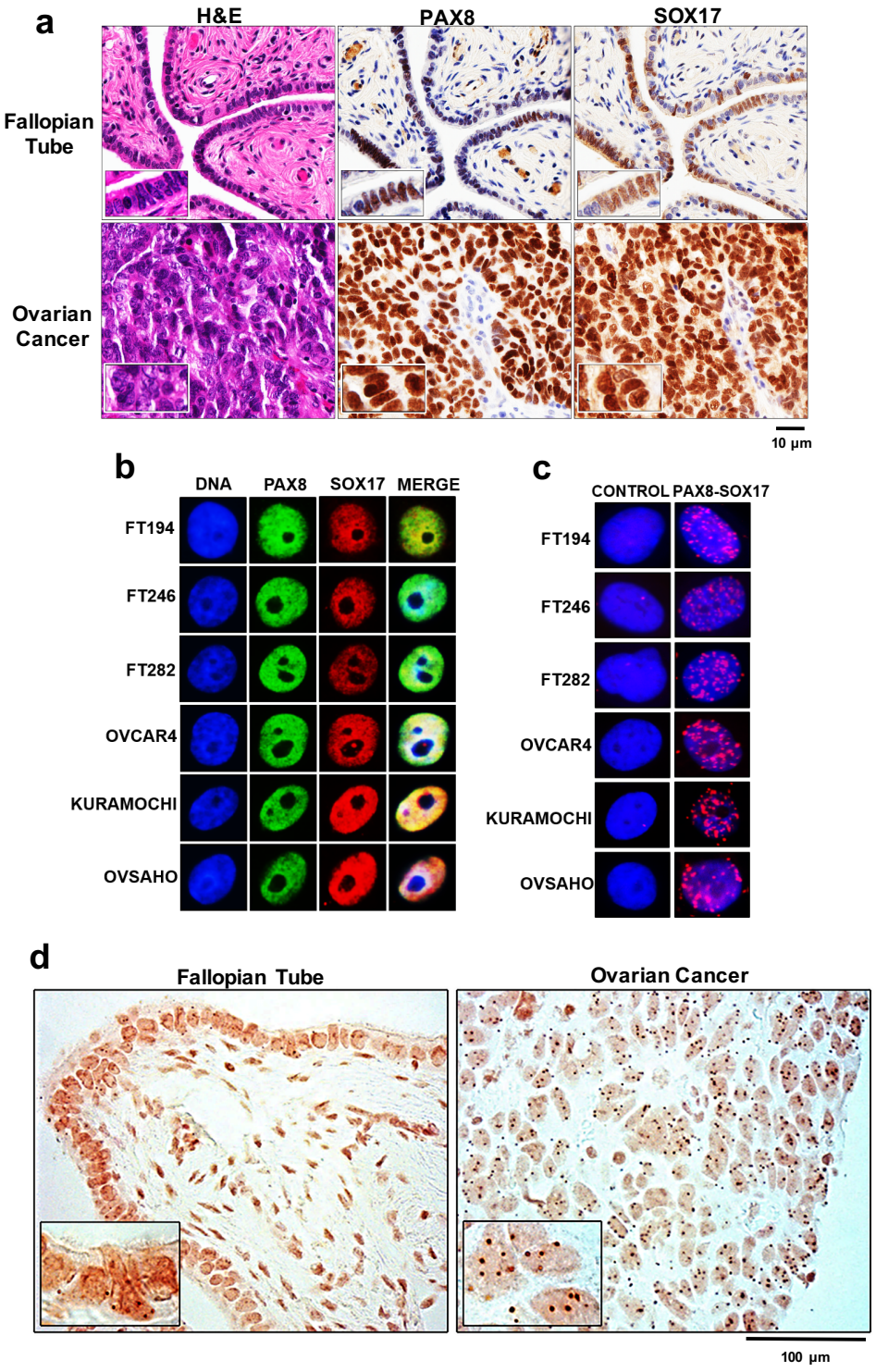

Figure 3: PAX8 and SOX17 are transcription co-regulators. (a-b) Immunoblot analyses following knockdown of PAX8 or SOX17 in FTSEC (FT194, FT246, and FT282) and in HGSOC (OVCAR4, KURAMOCHI, and OVSAHO) cells showing SOX17 expression dependency on PAX8 regulation. (c-d) Real-time PCR analysis following of PAX8 or SOX17 in FTSEC (FT194, FT246, and FT282) and in HGSOC (OVCAR4, KURAMOCHI, and OVSAHO) cells depicting the transcriptional co-regulation of SOX17 by PAX8. (e-f) Luciferase reporter assay using reporter with 5X PAX8-recognition sequence.

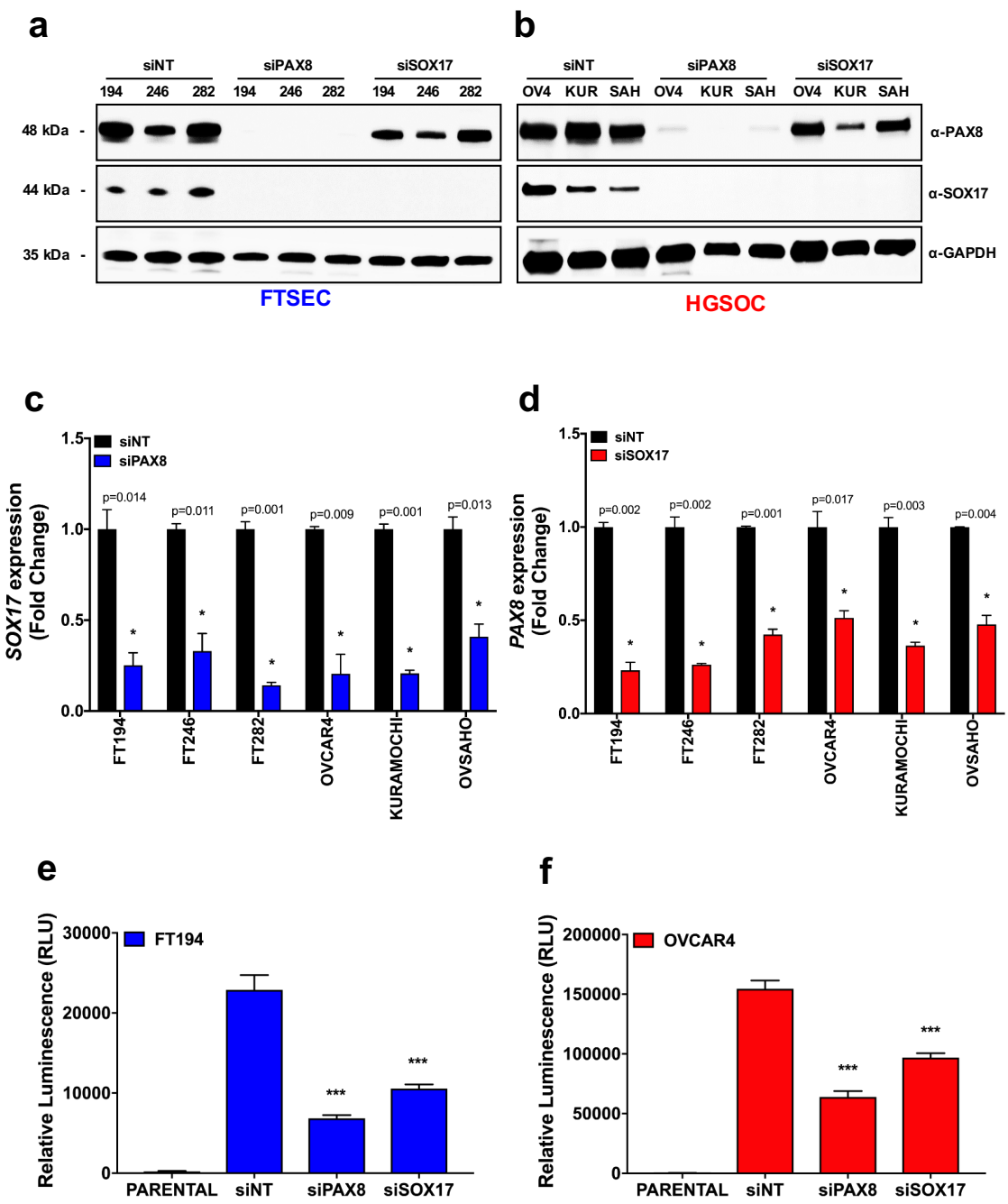

Figure 4: PAX8 and SOX17 regulate a common set of genes. (a) RNA-seq unsupervised clustering of PAX8, SOX17, and commonly regulated target genes. Profiles obtained with OVCAR4 after 72 hr knockdowns; fold change >1; $P < 0.05$. (b) Venn diagram representing number of genes up-regulated under each condition. (c) Ontology analysis of the PAX8-SOX17 commonly up-regulated genes. (d) RPPA unsupervised clustering of PAX8-SOX17 commonly regulated proteins. (e) Top-ranked PAX8-SOX17 commonly regulated proteins. (f) Immunoblot showing SERPINE1 up-regulation after PAX8 or SOX17 knockdown. (g) Real-time PCR showing *SERPINE1* up-regulation after PAX8 or SOX17 knockdown.

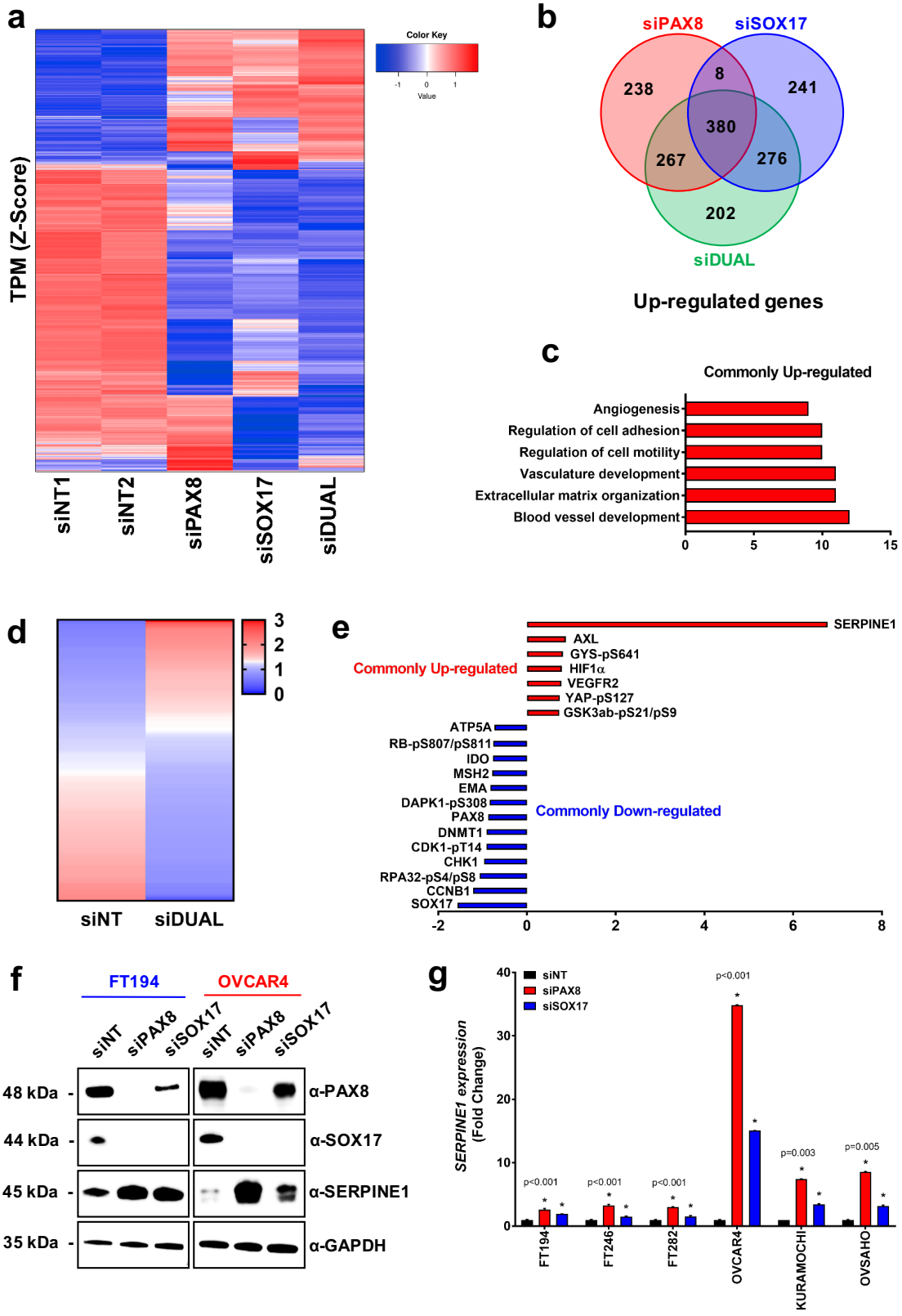

Figure 5: PAX8 and SOX17 regulate the secretion of angiogenesis mediators. (a) Human angiogenesis array of conditioned media from FTSEC and HGSOC cells following PAX8 or SOX17 knockdown. (b) Effect of PAX8 knockdown on specific analytes was produced by quantifying the array membrane spots intensity. (c) ELISA for quantification of secreted SERPINE1 in the FTSEC- and HGSOC-conditioned media. (d) ELISA for the quantitation of secreted VEGF in the FTSEC and HGSOC conditioned media. (e) ELISA showing SERPINE1 secreted by FTSEC and HGSOC. (f) ELISA experiments showing the effects of PAX8 or SOX17 knockdown on levels of SERPINE1 in HGSOC.

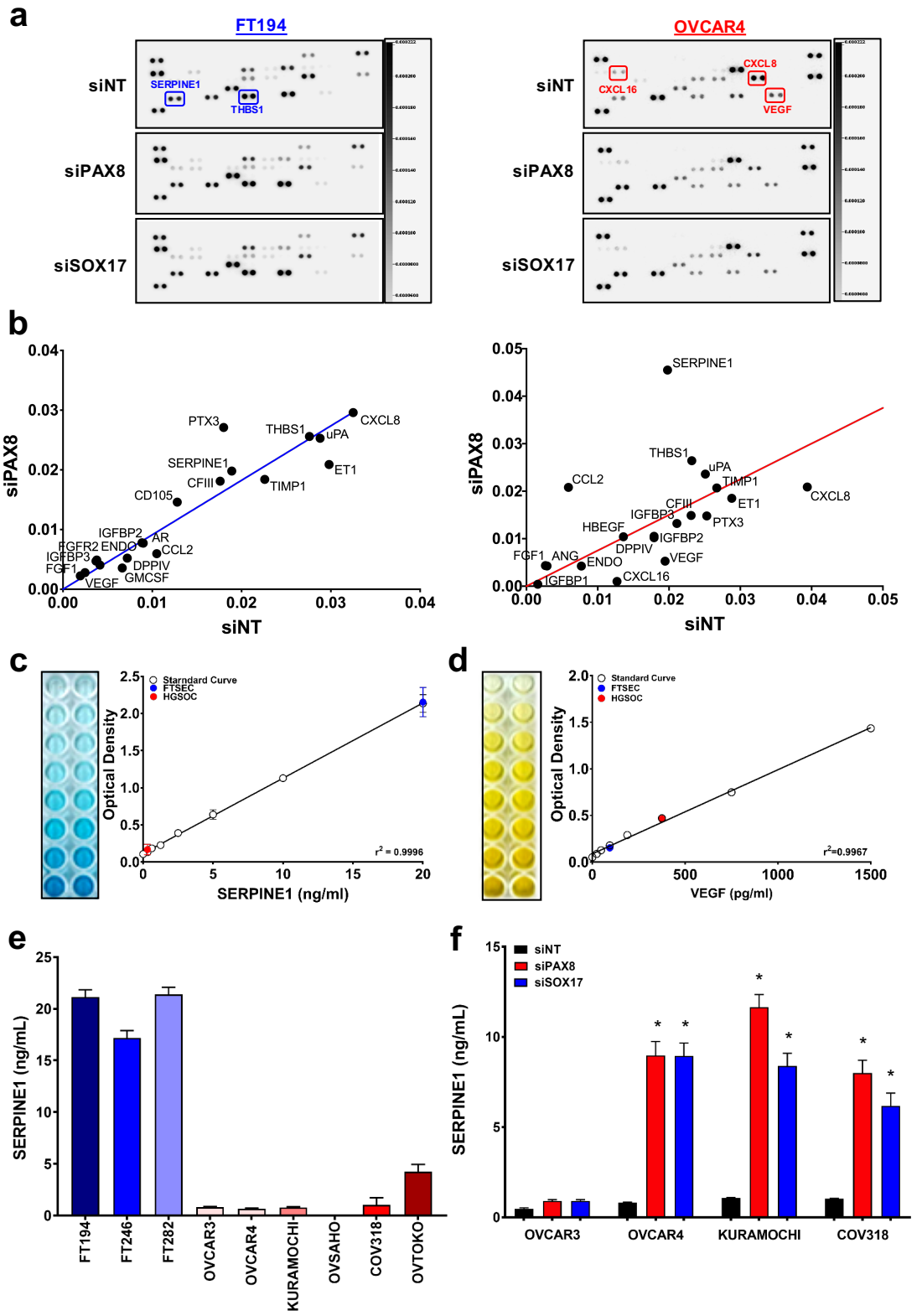

Figure 6: PAX8 and SOX17 promote ovarian cancer angiogenesis. (a) Endothelial cells tube formation assay. Representative images depict negative control, VEGF, SERPINE1, FTSEC, and HGSOC conditioned media after PAX8 or SOX17 knockdown. (b) Quantitation of the HUVEC neo-vessels loops. (c) Neovascularization in angioreactors containing conditioned media from HGSOC cells, but not from FTSEC after implantation in nude mice. (d) Quantitation of endothelial cell invasion into angioreactors.

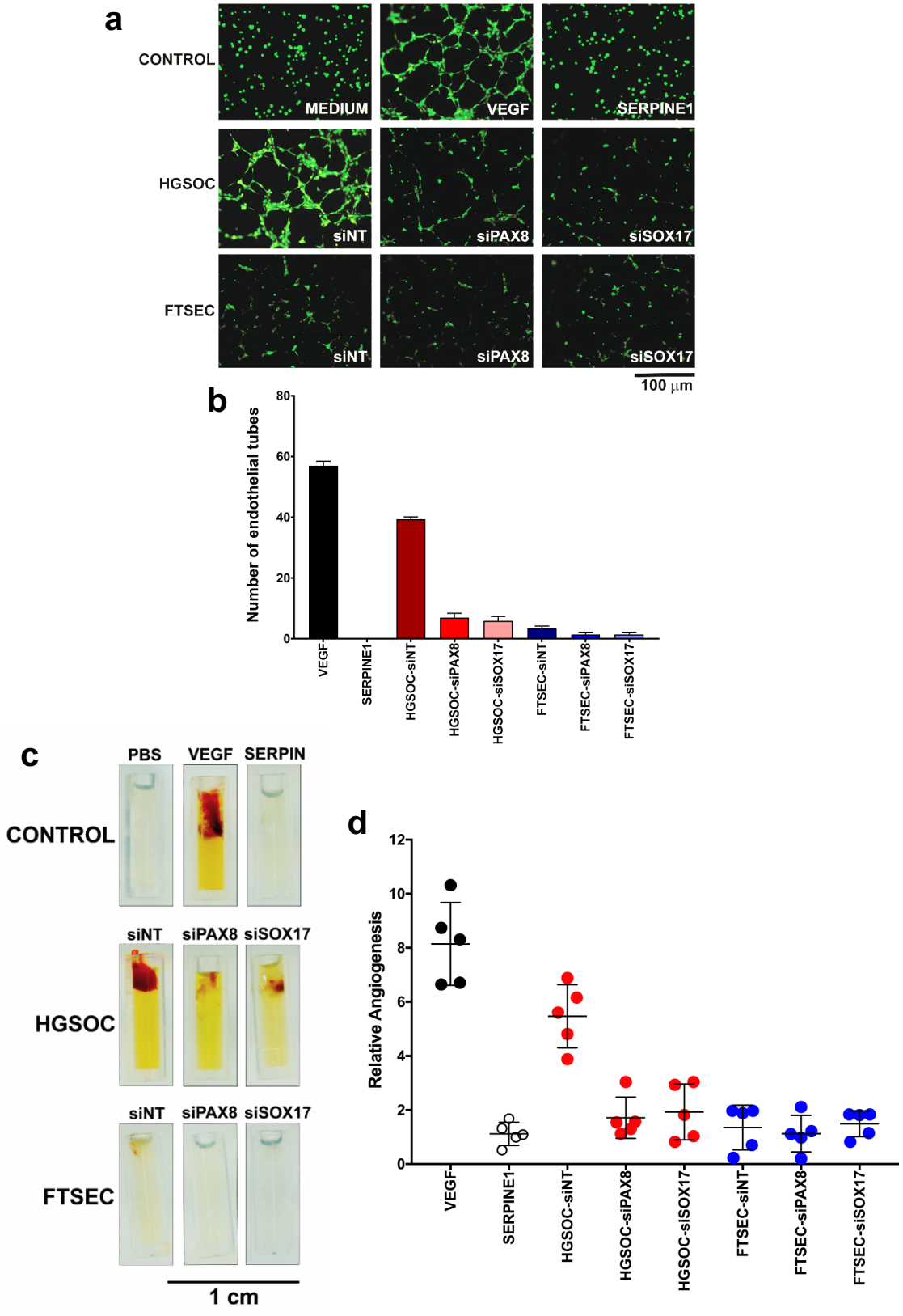

Figure 7: PAX8 or SOX17 doxycycline-inducible knockdown inhibits ovarian cancer progression. (a) Immunoblot of OVTOKO cells harboring inducible shPAX8 or shSOX17 before and after the induction with 1µg/ml of doxycycline. (b) *In vivo* imaging of OVTOKO tumors in NSG female mice. Animals were imaged after two weeks of doxycycline supplementation. (c) Necropsy of animals depicting ascites and tumors (white arrow) only in the non-targeting control group. (d) The volume of ascites collected from mice after two weeks of doxycycline supplementation. (e) NSG mice reproductive system depicting ovarian cancer volume.

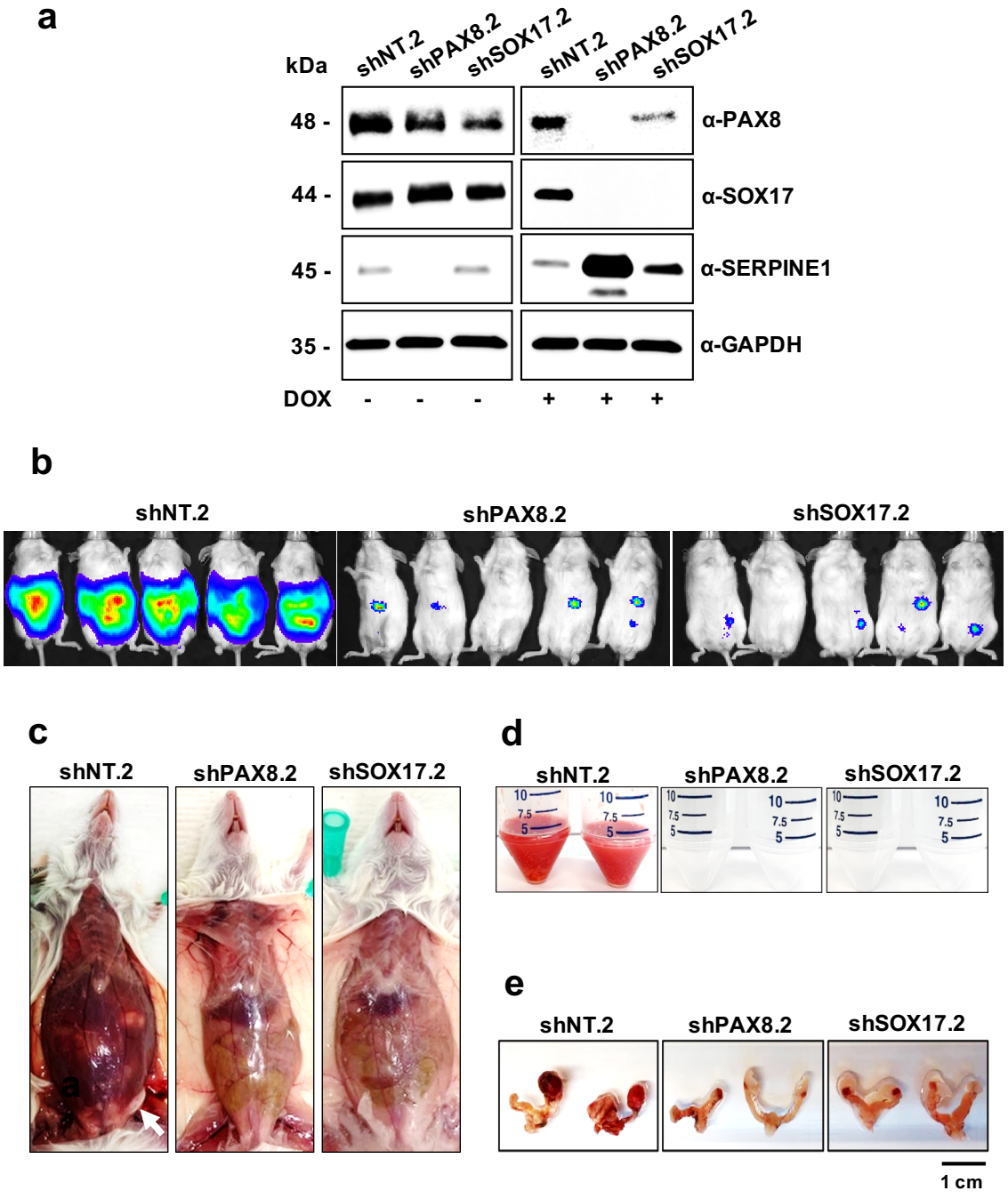

SUPPLEMENTAL INFORMATION

SI 1: PAX8 and SOX17 have a strong correlation and dependency on ovarian cancer. (a) TCGA ovarian cancer Pearson correlation of PAX8 with the newly identified PAX8-interacting partners. (b) SOX17 has the strongest correlation with PAX8 in ovarian cancer. (c) Ovarian carcinoma cells PAX8 dependency. (d) Ovarian carcinoma cells SOX17 dependency and (e) Ovarian carcinoma cells PAX8-SOX17 co-dependency.

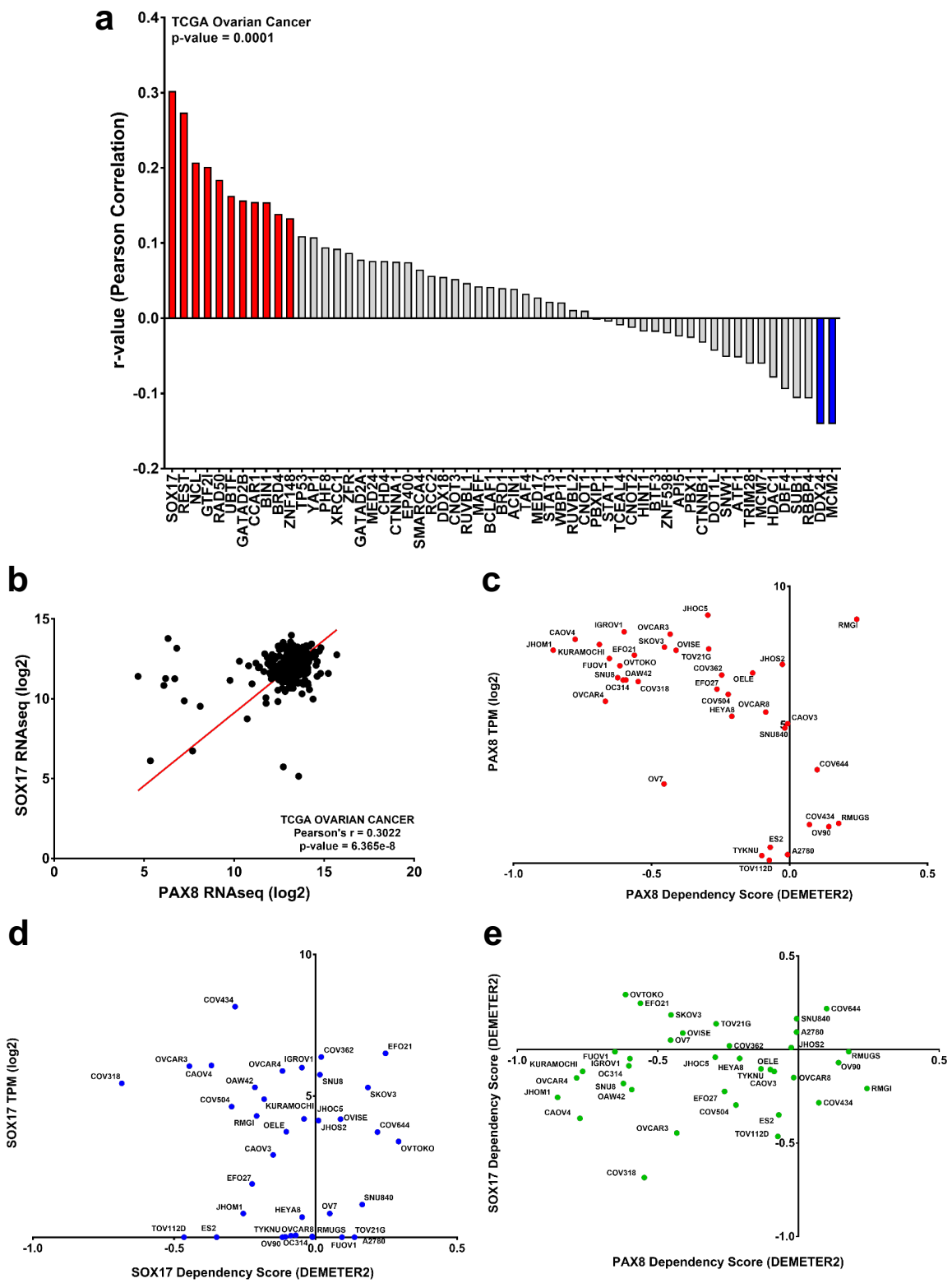

SI 2: Overexpression of PAX8 and SOX17 in ovarian carcinoma cases. (a) Higher expression of PAX8 in ovarian cancer samples. (b) Differential expression of SOX17 in ovarian cancer samples. (c) Most of the TCGA ovarian cancer samples have high PAX8 and SOX17 co-expression. (d) Higher number of PAX8-SOX17 interactions on ovarian cancer cell lines.

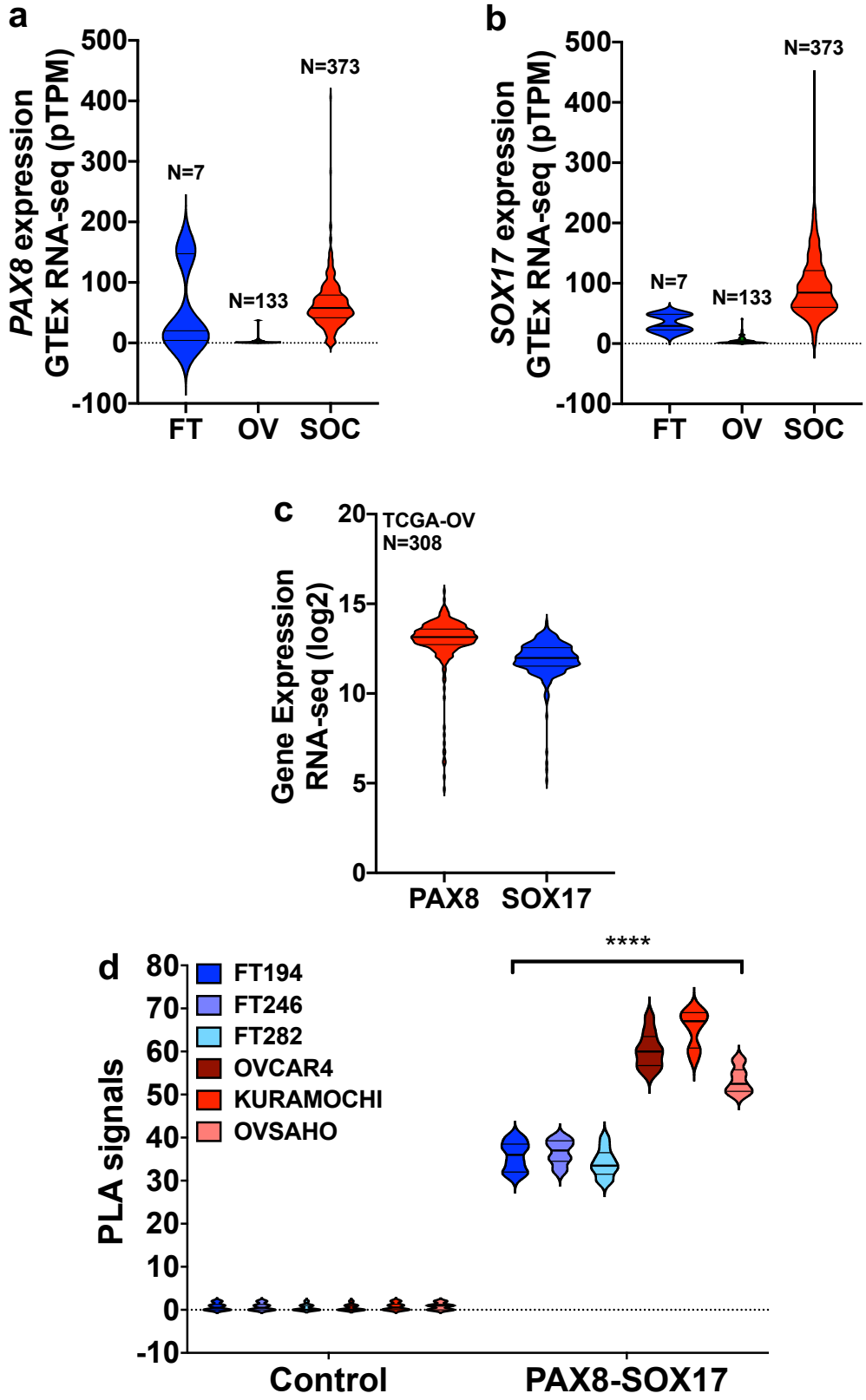

SI 3: PAX8-SOX17 expression co-regulation. (a-b) Immunoblot of four deconvoluted siPAX8 and four deconvoluted siSOX17 knockdowns on FTSEC and HGSOC cell lines. (c-d) PAX8 and SOX17 protein levels after knockdowns with four pooled siPAX8, four pooled siSOX17 or then all combined by reverse-phase protein array.

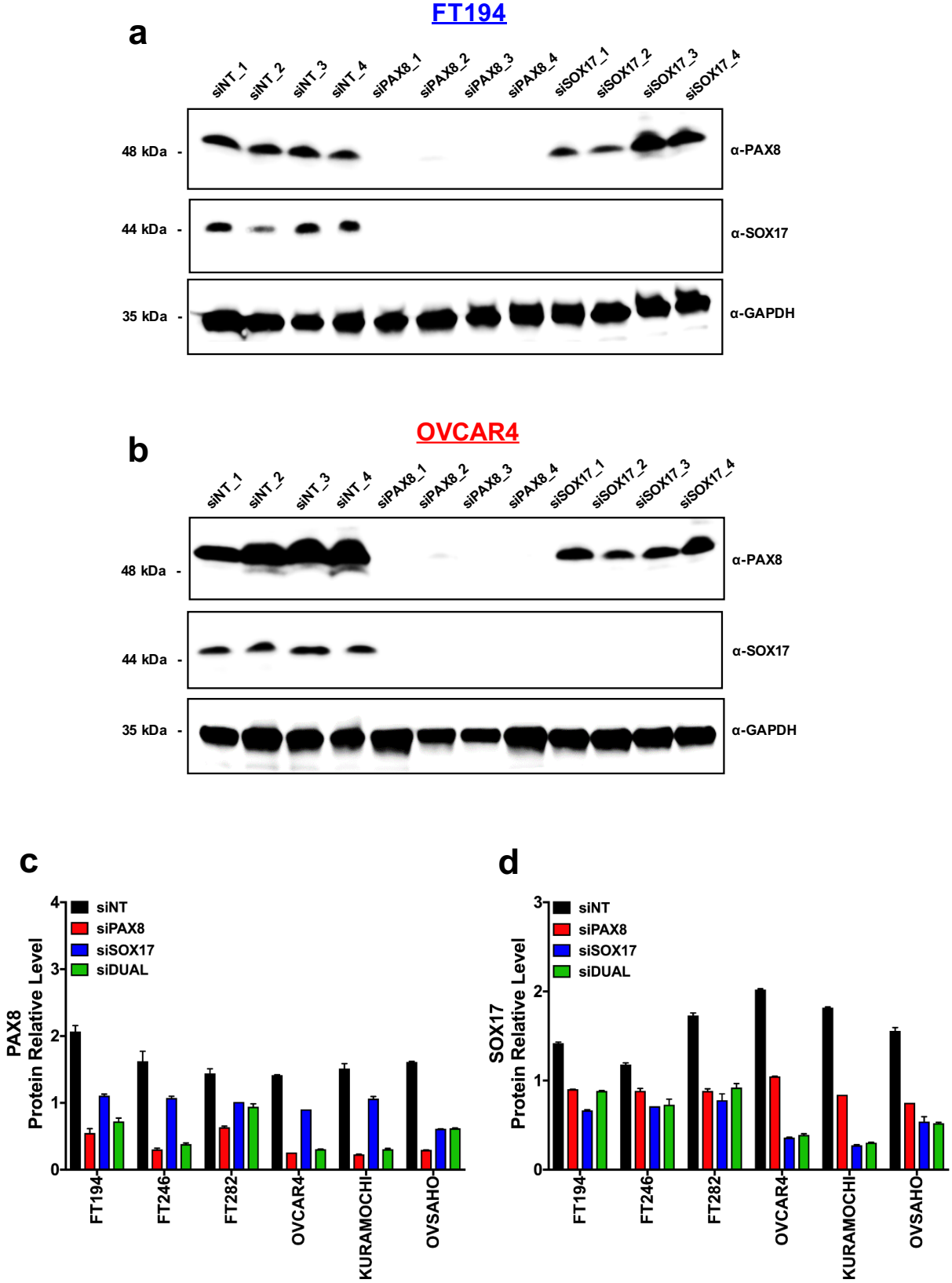

SI 4: PAX8-SOX17 tightly suppresses SERPINE1 expression. (a) RNA-seq analysis depicting *SERPINE1* gene up-regulation after PAX8, SOX17 or DUAL knockdown. (b) *SERPINE1* average expression after PAX8, SOX17 or DUAL knockdown. (c) RPPA ontology analysis corroborating enrichment of angiogenesis and VEGF pathways. (d) SERPINE1 relative protein levels in different FTSEC lines and HGSOC lines, depicting suppression of SERPINE1 during malignant transformation. (e) Immunoblot of different benign and malignant cell lines showing drastically reduction of SERPINE1 levels in cell lines with increased SOX17 expression.

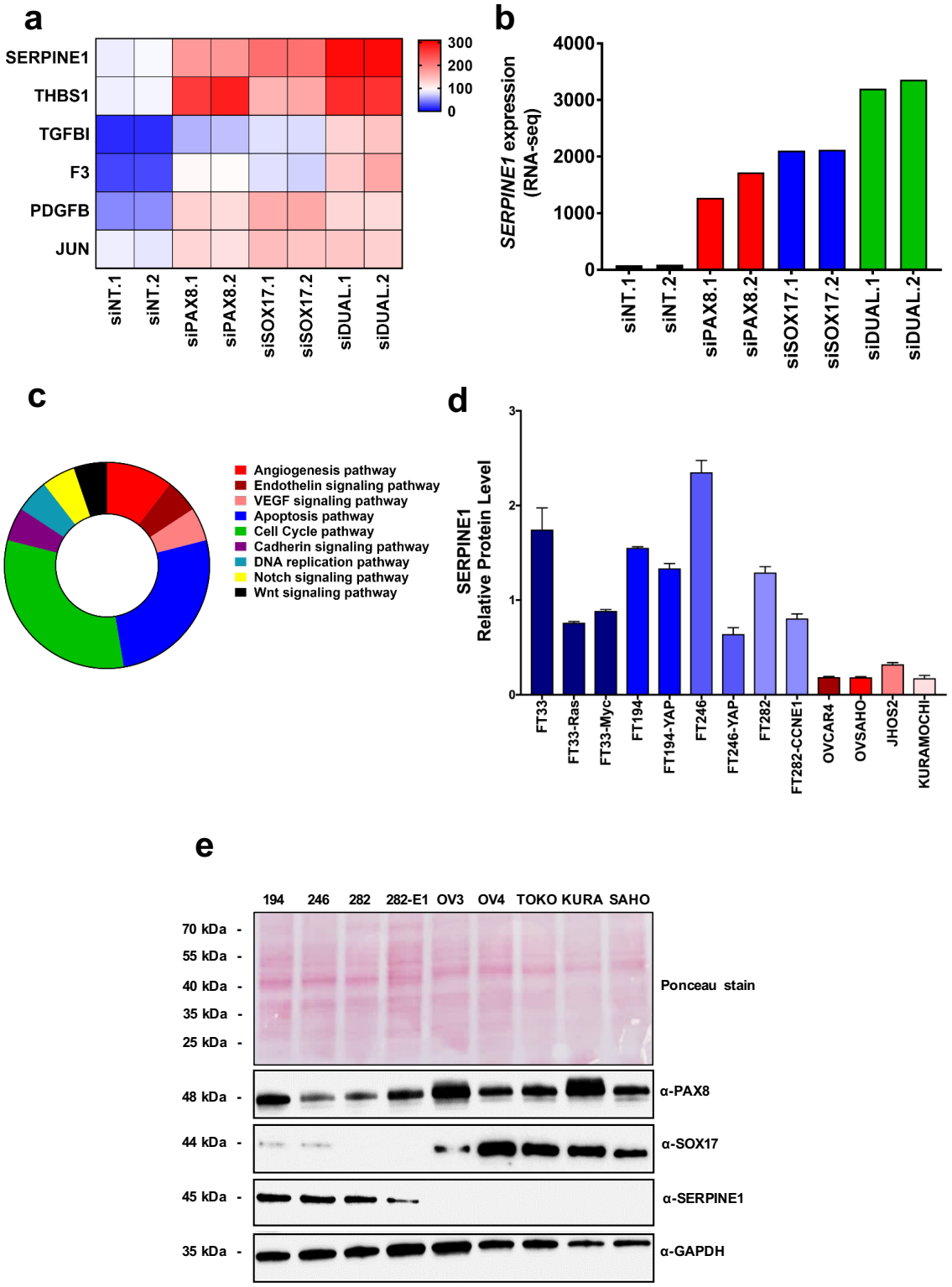

SI 5: PAX8 and SOX17 regulate the secretion of angiogenesis mediators. (a) Human angiogenesis arrays of fresh DMEM/F12 and RMPI media with no detection of angiogenesis mediators, negative controls. (b-c-d) Human angiogenesis array of additional three fallopian tube secretory cells and additional three ovarian carcinoma cells conditioned media after PAX8 or SOX17 knockdown.

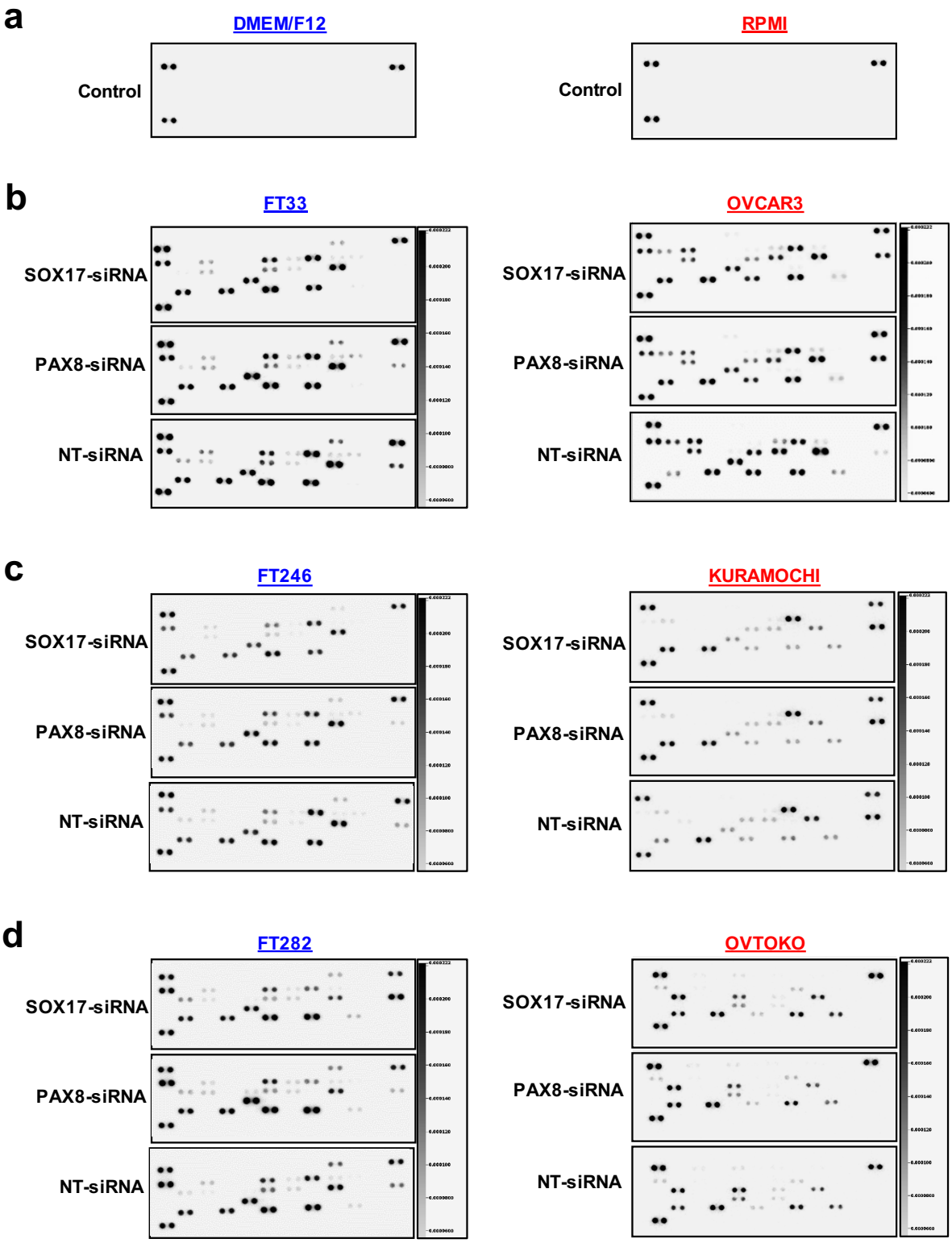

SI 6: PAX8-SOX17 regulates angiogenesis through the PLCy1 pathway. (a) Schematic illustration of the PLCy1 pathway. (b) RPPA analysis showing up-regulation of VEGFR2 protein levels followed PAX8 and SOX17 knockdown. (c) RPPA analysis showing reduced phosphorylated-PLCy1 and phosphorylated-ERK1/2 (active molecules) followed PAX8 and SOX17 knockdown. (d) Confirmation by western blot of the PLCy1 pathway inactivation.

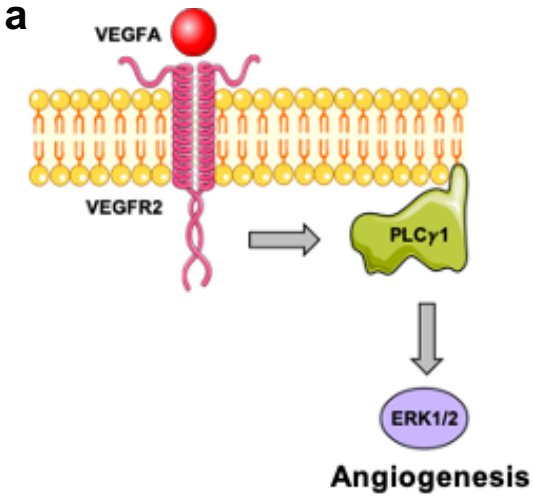

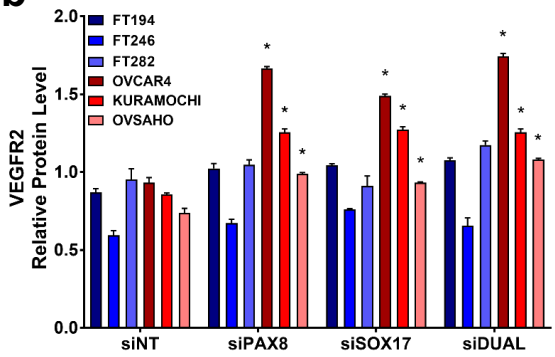

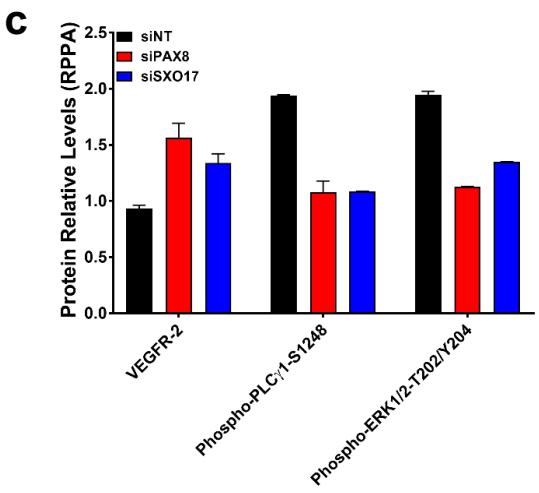

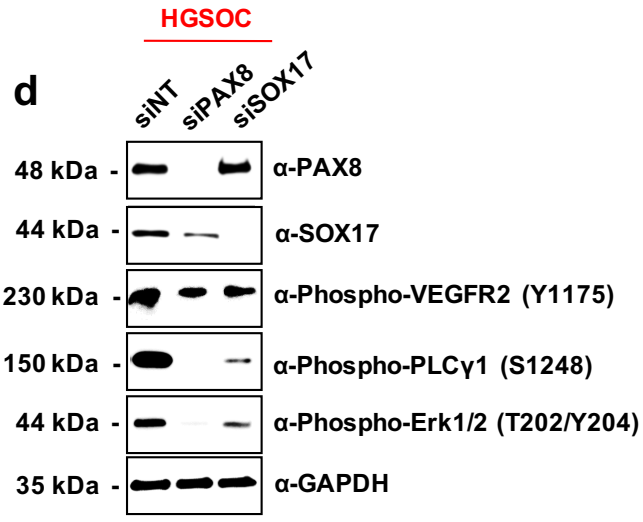

SI 7: PAX8-SOX17 suppress anti-angiogenesis factors. (a) Spearman correlation analysis of TCGA ovarian cancer data set depicting negative inversely correlation between SOX17 and angiogenesis inhibitors (SERPINE1 and THBS1). (b) Schematic diagram of the activation of tumor angiogenesis by PAX8 and SOX17 expression.

a

TCGA-OVARIAN	SOX17 vs. SERPINE1	SOX17 vs. THBS1
Spearman r	-0.3222	-0.2936
95% confidence interval	-0.4216 to -0.2152	-0.3952 to -0.1848
P value		
P (two-tailed)	<0.0001	<0.0001
P value summary	****	****
Significant? (alpha = 0.05)	Yes	Yes
Number of XY Pairs	308	308

b

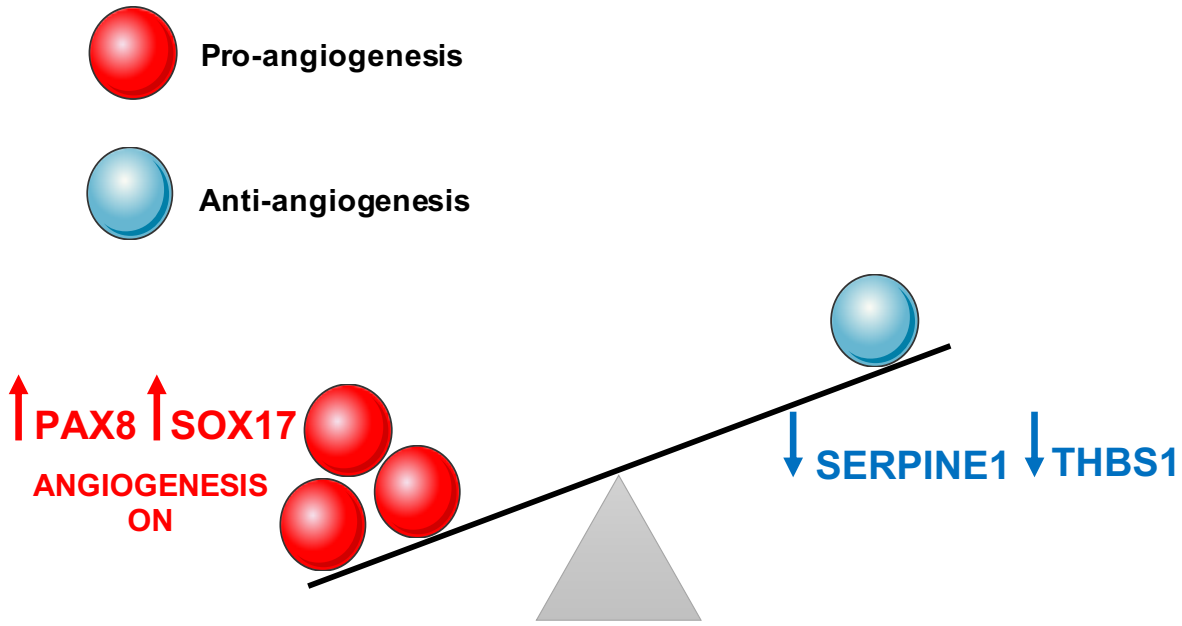

TABLES

Table 1: Putative PAX8-interacting partners.

UniProtKB Accession no.	Spot name	Description	Theoretical mass (kDa)	MaxQuant search results			Fold change Cancer *vs.* Normal[#]
				No. of matched peptides	Sequence coverage (%)	Score	
TRANSCRIPTION FACTORS AND REGULATORS							
Q06710	PAX8	Paired box protein PAX-8	48.2	13	33.8	162.9	+1.38
Q13263	TRIM28	Transcription intermediary factor 1-beta	88.5	5	11.3	79.4	-0.22
Q1MSW8	TP53	Cellular tumor antigen p53	50.2	4	22.2	76.1	+2.79
Q9H6I2	SOX17	Transcription factor SOX-17	44.3	3	11.1	74.8	+1.05
P78347	GTF2I	General transcription factor III	107.9	19	11.3	73.3	+1.06
Q86YP4	GATAD2A	Transcriptional repressor p66-alpha	68.1	7	9.6	45.1	-0.66
P40763	STAT3	Signal transducer and activator of transcription 3	76.1	8	3.9	39.6	+0.01
A5YKK6	CNOT1	CCR4-NOT transcription complex subunit 1	266.4	6	2.5	38.1	-1.13
P17480	UBTF	Nucleolar transcription factor 1	75.9	10	6.3	31.6	-0.96
P51532	SMARCA4	Transcription activator BRG1	184.6	15	3.9	28.8	-0.18
O00268	TAF4	Transcription initiation factor TFIID subunit 4	50.2	3	6.8	20.4	+0.70
O60885	BRD4	Bromodomain-containing protein 4	152.2	3	2.5	18.7	-2.08
Q13573	SNW1	SNW domain-containing protein 1	43.3	3	9.9	18.1	+1.57
O75448	MED24	Mediator of RNA polymerase II transcription subunit 24	91.3	3	4.6	17.8	-0.79
Q9NZN8	CNOT2	CCR4-NOT transcription complex subunit 2	29.9	2	9.1	16.7	-0.97
P20290	BTF3	Transcription factor BTF3	17.7	2	17.3	14.6	+2.02
A0A0U1RRM1	GATAD2B	Transcriptional repressor p66-beta	63.4	4	5.9	14.2	-0.30
E9PJZ4	MED17	Mediator of RNA polymerase II transcription subunit 17	16.3	2	16.1	13.8	+1.94
Q96EI5	TCEAL4	Transcription elongation factor A protein-like 4	21.5	5	11.8	12.5	0.00
H3BQQ2	ZNF598	Zinc finger protein 598	93.3	4	1.5	12.5	+0.34

Q9NYF8	BCLAF1	Bcl-2-associated transcription factor 1	52.9	11	5.4	12.2	-0.23
O75175	CNOT3	CCR4-NOT transcription complex subunit 3	31.2	8	16.3	10.9	-4.48
Q4FD37	ZNF148	Zinc finger protein 148	74.5	4	1.2	9.2	0.00
Q96AQ6	PBXIP1	Pre-B-cell leukemia transcription factor-interacting protein 1	57.5	6	2.2	8.5	+0.65
P42224	STAT1	Signal transducer and activator of transcription 1-alpha/beta	88.3	3	1.7	8.1	-0.93
Q9ULX9	MAFF	Transcription factor MafF	14.5	2	11.9	7.5	0.00
Q13127	REST	RE1-silencing transcription factor	52.2	3	2.1	7.3	+1.02
P46937	YAP1	Transcriptional coactivator YAP1	18.7	9	6.5	6.6	+1.27
P53999	SUB1	Activated RNA polymerase II transcriptional coactivator p15	14.4	3	18.9	6.4	+1.90
P40424	PBX1	Pre-B-cell leukemia transcription factor 1	46.6	1	10.3	5.8	+0.78
P18846	ATF1	Cyclic AMP-dependent transcription factor ATF-1	57.6	23	5.8	2.1	+0.03
RNA PROCESSING							
Q9BQ02	NCL	Nucleolin	76.6	11	30.1	188.9	-0.63
A8K849	ZFR	Zinc finger RNA-binding protein	66.3	3	7.1	16.6	+0.41
Q9NVP1	DDX18	ATP-dependent RNA helicase DDX18	61.6	4	4.4	13.9	+2.24
Q59FS7	DDX24	ATP-dependent RNA helicase DDX24	75.1	1	1.6	8.4	+5.29
Q9Y2W2	WBP11	WW domain-binding protein 11	64.9	1	2.4	7.2	+0.93
DNA PROCESSING							
P33993	MCM7	DNA replication licensing factor MCM7	81.2	11	23.8	114.6	+0.35
Q92878	RAD50	DNA repair protein RAD50	138.4	12	11.5	85.4	+0.49
Q9Y265	RUVBL1	RuvB-like 1	50.2	8	25.4	76.1	+1.46
Q14839	CHD4	Chromodomain-helicase-DNA-binding protein 4	215.2	15	3.6	45.8	+0.18
Q9P258	RCC2	Protein RCC2	56.1	5	14.2	43.2	+1.53
Q9Y230	RUVBL2	RuvB-like 2	51.1	9	13.2	35.4	+0.84
P49736	MCM2	DNA replication licensing factor MCM2	87.4	6	6.1	26.2	-0.09
P18887	XRCC1	DNA repair protein XRCC1	42.8	2	5.8	13.5	-1.03
B7Z8C6	DBF4	Protein DBF4 homolog A	51.8	2	3.1	6.5	+1.75
EPIGENETIC REGULATORS							
Q09028	RBBP4	Histone-binding protein RBBP4	46.9	4	7.9	27.9	-2.96

O94776	MTA2	Metastasis-associated protein MTA2	75.0	3	3	12.5	+0.03
Q6IT96	HDAC1	Histone deacetylase	55.1	2	4.4	11.8	+1.99
Q96L91	EP400	E1A-binding protein p400	335.8	1	0.6	9.4	+0.31
Q8TEK3	DOT1L	Histone-lysine N-methyltransferase, H3 lysine-79 specific	24.1	3	3.4	7.6	-1.60
Q9UPP1	PHF8	Histone lysine demethylase PHF8	33.2	1	4.5	7.2	-0.27
Q13330	MTA1	Metastasis-associated protein MTA1	28.7	8	5.1	6.3	+1.55
Q59G93	BRD1	Bromodomain-containing protein 1	53.8	1	1.9	6.2	+0.30
APOPTOTIC SIGNALING PATHWAY							
Q8N163	CCAR2	Cell cycle and apoptosis regulator protein 2	102.9	8	10.2	57.1	+0.51
Q8IX12	CCAR1	Cell division cycle and apoptosis regulator protein 1	131.4	5	3.1	30.9	+1.56
Q9BZZ5	API5	Apoptosis inhibitor 5	37.5	4	10.0	27.2	+2.22
Q9UKV3	ACIN1	Apoptotic chromatin condensation inducer in the nucleus	122.5	3	3.8	19.9	-2.24
D6RC06	HINT1	Histidine triad nucleotide-binding protein 1	7.3	1	21.5	6.7	+0.84
TRANSFORMATION SIGNALING PATHWAY							
G3XAM7	CTNNA1	Catenin alpha-1	92.7	6	8.8	76.4	-1.01
B4DSW9	CTNNB1	Catenin beta-1	77.5	3	3.9	24.3	+0.13
O00499	BIN1	Myc box-dependent-interacting protein 1	43.2	1	3.6	6.3	-1.12

[#]Average ratio between the Cancer and Normal cells are reported and significant values indicated (*p < 0.05).

Table 2: Top PAX8-SOX17 commonly regulated genes.

COMMONLY UP-REGULATED TARGET GENES		COMMONLY DOWN-REGULATED TARGET GENES	
Gene	**Log-fold change**	**Gene**	**Log-fold change**
SERPINE1	5.54863858	PYY	-8.0262675
IL11	5.27536243	TMEM101	-5.7263682
NPPB	5.18800181	FGF18	-5.4123449
KLK5	4.50271261	TGM7	-4.9926057
FGF1	4.4055198	CA2	-4.8188457
CPA4	4.32537639	CCNA1	-4.5055642
MYL7	3.80515773	CXCL5	-4.409147
ADAMTSL4	3.79017684	FOXQ1	-4.3460707
FILIP1L	3.64159103	NOTUM	-4.3070766
HBEGF	3.62339664	GBP5	-4.2098481
TGFBI	3.61350996	TMEM171	-4.1579087
RASD2	3.52832382	ZBED6CL	-4.0422849
PMEPA1	3.48254273	BMPER	-3.7191215
SEMA3C	3.43402726	FST	-3.4878197
DYSF	3.32114739	ATP2B2	-3.4437388
ITGA2	3.314082	LRRC61	-3.441764
CYP1B1	3.28587766	RHOC	-3.4246182
NCF2	3.26470577	MYB	-3.4111303
ABCC3	3.21212074	NMU	-3.4026155
DAB2	3.18763588	PRRX2	-3.3958186
CA9	3.17582117	TXK	-3.3917272
CD274	3.17245293	AGMAT	-3.3704743
CSF1R	3.16372011	CTTNBP2	-3.3622138
AKR1B10	3.09123637	IQGAP2	-3.300818
SULT2B1	3.0772257	KLHL14	-3.2936874
PDCD1LG2	3.06482259	LRRC41	-3.290006
PCP4L1	3.05895596	IMPDH1	-3.285422

[#] Top significant gene expression changes p-values < 0.01.

Table 3: PAX8-SOX17 significantly co-regulated target proteins

UP-REGULATED TARGET PROTEINS			DOWN-REGULATED TARGET PROTEINS		
Protein	**Difference**	**t-ratio**	**Protein**	**Difference**	**t-ratio**
SERPINE1	6.772	74.24	SOX17	-1.563	17.13
Axl	0.8736	9.577	Cyclin-B1	-1.211	13.27
Gys_pS641	0.8122	8.903	RPA32_pS4_pS8	-1.069	11.71
Hif-1-alpha	0.7834	8.589	Chk1	-0.9642	10.57
VEGFR-2	0.7769	8.517	CDK1_pT14	-0.9087	9.961
YAP_pS127	0.7397	8.109	DNMT1	-0.9073	9.946
GSK-3a-b_pS21_pS9	0.7283	7.984	PAX8	-0.8738	9.579
ATR	0.7	7.674	DAPK1_pS308	-0.8424	9.235
Connexin-43	0.6899	7.563	EMA	-0.8236	9.029
HSP27_pS82	0.6696	7.34	MSH2	-0.7811	8.563
B7-H4	0.6279	6.884	IDO	-0.766	8.398
GSK-3B	0.6189	6.785	Rb_pS807_pS811	-0.7593	8.323
NDRG1_pT346	0.6089	6.676	ATP5A	-0.7315	8.019
MLKL	0.573	6.281	ENY2	-0.7228	7.924
G6PD	0.5712	6.262	Rheb	-0.7226	7.921
p21	0.5468	5.995	PARP	-0.7224	7.919
Atg7	0.5453	5.978	Ets-1	-0.6919	7.585
MCT4	0.538	5.898	MSH6	-0.6902	7.566
Stat3	0.5376	5.894	Slfn11	-0.6349	6.96
HMHA1	0.515	5.646	RBM15	-0.6324	6.933
PEA-15	0.5141	5.636	PLK1	-0.615	6.743
Rab25	0.5075	5.563	BRD4	-0.5906	6.474
Src_pY416	0.5015	5.498	cdc25C	-0.5894	6.461
A-Raf	0.4957	5.435	Cdc6	-0.575	6.303
INPP4b	0.4906	5.378	FOXM1	-0.5734	6.286
E-Cadherin	0.4877	5.346	p53	-0.5685	6.233
Gys	0.4875	5.344	Chk2	-0.5643	6.186
SHP-2_pY542	0.4854	5.321	UQCRC2	-0.5319	5.831
Merlin	0.4832	5.297	AMPKa_pT172	-0.5024	5.508
TRIM25	0.4789	5.25	Rad50	-0.4901	5.372
Coup-TFII	0.4624	5.069	GATA3	-0.4884	5.354
Paxillin	0.4544	4.981	PYGM	-0.474	5.196
NQO1	0.4418	4.843	KAP1	-0.4675	5.126
S6_pS235_pS236	0.4356	4.775	eEF2	-0.4655	5.103
Mitofusin-2	0.4326	4.742	c-Abl_pY412	-0.4479	4.91
Atg5	0.4267	4.678	Aurora-A	-0.4457	4.886

[#] Top significant relative protein changes p-values < 0.01.

REFERENCES

1. Siegel RL, Miller KD, and Jemal A. Cancer statistics, 2019. *CA Cancer J Clin.* 2019;69(1):7-34.

2. Ferlay J, Colombet M, Soerjomataram I, Mathers C, Parkin DM, Pineros M, et al. Estimating the global cancer incidence and mortality in 2018: GLOBOCAN sources and methods. *Int J Cancer.* 2019;144(8):1941-53.

3. Reid BM, Permuth JB, and Sellers TA. Epidemiology of ovarian cancer: a review. *Cancer Biol Med.* 2017;14(1):9-32.

4. Torre LA, Trabert B, DeSantis CE, Miller KD, Samimi G, Runowicz CD, et al. Ovarian cancer statistics, 2018. *CA Cancer J Clin.* 2018;68(4):284-96.

5. Perets R, and Drapkin R. It's Totally Tubular....Riding The New Wave of Ovarian Cancer Research. *Cancer Res.* 2016;76(1):10-7.

6. Ducie J, Dao F, Considine M, Olvera N, Shaw PA, Kurman RJ, et al. Molecular analysis of high-grade serous ovarian carcinoma with and without associated serous tubal intra-epithelial carcinoma. *Nat Commun.* 2017;8(1):990.

7. Labidi-Galy SI, Papp E, Hallberg D, Niknafs N, Adleff V, Noe M, et al. High grade serous ovarian carcinomas originate in the fallopian tube. *Nat Commun.* 2017;8(1):1093.

8. Wu RC, Wang P, Lin SF, Zhang M, Song Q, Chu T, et al. Genomic landscape and evolutionary trajectories of ovarian cancer precursor lesions. *J Pathol.* 2019;248(1):41-50.

9. Eckert MA, Pan S, Hernandez KM, Loth RM, Andrade J, Volchenboum SL, et al. Genomics of Ovarian Cancer Progression Reveals Diverse Metastatic Trajectories Including Intraepithelial Metastasis to the Fallopian Tube. *Cancer Discov.* 2016;6(12):1342-51.

10. Sherman-Baust CA, Kuhn E, Valle BL, Shih Ie M, Kurman RJ, Wang TL, et al. A genetically engineered ovarian cancer mouse model based on fallopian tube transformation mimics human high-grade serous carcinoma development. *J Pathol.* 2014;233(3):228-37.

11. McCool KW, Freeman ZT, Zhai Y, Wu R, Hu K, Liu CJ, et al. Murine Oviductal High-Grade Serous Carcinomas Mirror the Genomic Alterations, Gene Expression Profiles, and Immune Microenvironment of Their Human Counterparts. *Cancer Res.* 2020;80(4):877-89.

12. Kim J, Coffey DM, Creighton CJ, Yu Z, Hawkins SM, and Matzuk MM. High-grade serous ovarian cancer arises from fallopian tube in a mouse model. *Proc Natl Acad Sci U S A.* 2012;109(10):3921-6.

13. Stuckelberger S, and Drapkin R. Precious GEMMs: emergence of faithful models for ovarian cancer research. *J Pathol.* 2018;245(2):129-31.

14. Mittag J, Winterhager E, Bauer K, and Grummer R. Congenital hypothyroid female pax8-deficient mice are infertile despite thyroid hormone replacement therapy. *Endocrinology.* 2007;148(2):719-25.

15. Mayran A, Pelletier A, and Drouin J. Pax factors in transcription and epigenetic remodelling. *Semin Cell Dev Biol.* 2015;44:135-44.

16. Laury AR, Perets R, Piao H, Krane JF, Barletta JA, French C, et al. A comprehensive analysis of PAX8 expression in human epithelial tumors. *Am J Surg Pathol.* 2011;35(6):816-26.

17. Perets R, Wyant GA, Muto KW, Bijron JG, Poole BB, Chin KT, et al. Transformation of the fallopian tube secretory epithelium leads to high-grade serous ovarian cancer in Brca;Tp53;Pten models. *Cancer Cell.* 2013;24(6):751-65.

18. Maniati E, Berlato C, Gopinathan G, Heath O, Kotantaki P, Lakhani A, et al. Mouse Ovarian Cancer Models Recapitulate the Human Tumor Microenvironment and Patient Response to Treatment. *Cell Rep.* 2020;30(2):525-40 e7.

19. Di Palma T, Filippone MG, Pierantoni GM, Fusco A, Soddu S, and Zannini M. Pax8 has a critical role in epithelial cell survival and proliferation. *Cell Death Dis.* 2013;4:e729.

20. Ghannam-Shahbari D, Jacob E, Kakun RR, Wasserman T, Korsensky L, Sternfeld O, et al. PAX8 activates a p53-p21-dependent pro-proliferative effect in high grade serous ovarian carcinoma. *Oncogene.* 2018;37(17):2213-24.

21. Rodgers LH, E Oh, Young AN, and Burdette JE. Loss of PAX8 in high-grade serous ovarian cancer reduces cell survival despite unique modes of action in the fallopian tube and ovarian surface epithelium. *Oncotarget.* 2016;7(22):32785-95.

22. Elias KM, Emori MM, Westerling T, Long H, Budina-Kolomets A, Li F, et al. Epigenetic remodeling regulates transcriptional changes between ovarian cancer and benign precursors. *JCI Insight.* 2016;1(13).

23. Corona RI, Seo JH, Lin X, Hazelett DJ, Reddy J, Fonseca MAS, et al. Non-coding somatic mutations converge on the PAX8 pathway in ovarian cancer. *Nat Commun.* 2020;11(1):2020.

24. Garcia-Heredia JM, Verdugo Sivianes EM, Lucena-Cacace A, Molina-Pinelo S, and Carnero A. Numb-like (NumbL) downregulation increases tumorigenicity, cancer stem cell-like properties and resistance to chemotherapy. *Oncotarget.* 2016;7(39):63611-28.

25. Allen HF, Wade PA, and Kutateladze TG. The NuRD architecture. *Cell Mol Life Sci.* 2013;70(19):3513-24.

26. Bohm M, Wachtel M, Marques JG, Streiff N, Laubscher D, Nanni P, et al. Helicase CHD4 is an epigenetic coregulator of PAX3-FOXO1 in alveolar rhabdomyosarcoma. *J Clin Invest.* 2016;126(11):4237-49.

27. Grimley E, Liao C, Ranghini EJ, Nikolovska-Coleska Z, and Dressler GR. Inhibition of Pax2 Transcription Activation with a Small Molecule that Targets the DNA Binding Domain. *ACS Chem Biol.* 2017;12(3):724-34.

28. De Palma M, Biziato D, and Petrova TV. Microenvironmental regulation of tumour angiogenesis. *Nat Rev Cancer.* 2017;17(8):457-74.

29. Zhou H, Yang YH, and Basile JR. Characterization of the Effects of Semaphorin 4D Signaling on Angiogenesis. *Methods Mol Biol.* 2017;1493:429-41.

30. Zhou H, Yang YH, Binmadi NO, Proia P, and Basile JR. The hypoxia-inducible factor-responsive proteins semaphorin 4D and vascular endothelial growth factor promote tumor growth and angiogenesis in oral squamous cell carcinoma. *Exp Cell Res.* 2012;318(14):1685-98.

31. Shi K, Yin X, Cai MC, Yan Y, Jia C, Ma P, et al. PAX8 regulon in human ovarian cancer links lineage dependency with epigenetic vulnerability to HDAC inhibitors. *Elife.* 2019;8.

32. Grimm D, Bauer J, Wise P, Kruger M, Simonsen U, Wehland M, et al. The role of SOX family members in solid tumours and metastasis. *Semin Cancer Biol.* 2019.

33. Hou L, Srivastava Y, and Jauch R. Molecular basis for the genome engagement by Sox proteins. *Semin Cell Dev Biol.* 2017;63:2-12.

34. Wilson M, and Koopman P. Matching SOX: partner proteins and co-factors of the SOX family of transcriptional regulators. *Curr Opin Genet Dev.* 2002;12(4):441-6.

35. Lang D, and Epstein JA. Sox10 and Pax3 physically interact to mediate activation of a conserved c-RET enhancer. *Hum Mol Genet.* 2003;12(8):937-45.

36. Mascarenhas JB, Littlejohn EL, Wolsky RJ, Young KP, Nelson M, Salgia R, et al. PAX3 and SOX10 activate MET receptor expression in melanoma. *Pigment Cell Melanoma Res.* 2010;23(2):225-37.

37. Zhang S, Bell E, Zhi H, Brown S, Imran SAM, Azuara V, et al. OCT4 and PAX6 determine the dual function of SOX2 in human ESCs as a key pluripotent or neural factor. *Stem Cell Res Ther.* 2019;10(1):122.

38. Ooki A, Dinalankara W, Marchionni L, Tsay JJ, Goparaju C, Maleki Z, et al. Epigenetically regulated PAX6 drives cancer cells toward a stem-like state via GLI-SOX2 signaling axis in lung adenocarcinoma. *Oncogene.* 2018;37(45):5967-81.

39. Reddy J, Fonseca MAS, Corona RI, Nameki R, Dezem FS, Klein IA, et al. Predicting master transcription factors from pan-cancer expression data. *bioRxiv 839142.* 2019.

40. Yang H, Lee S, Lee S, Kim K, Yang Y, Kim JH, et al. Sox17 promotes tumor angiogenesis and destabilizes tumor vessels in mice. *J Clin Invest.* 2013;123(1):418-31.

41. Lee SH, Lee S, Yang H, Song S, Kim K, Saunders TL, et al. Notch pathway targets proangiogenic regulator Sox17 to restrict angiogenesis. *Circ Res.* 2014;115(2):215-26.

42. Ramasamy SK, Kusumbe AP, Wang L, and Adams RH. Endothelial Notch activity promotes angiogenesis and osteogenesis in bone. *Nature.* 2014;507(7492):376-80.

43. Pitulescu ME, Schmidt I, Giaimo BD, Antoine T, Berkenfeld F, Ferrante F, et al. Dll4 and Notch signalling couples sprouting angiogenesis and artery formation. *Nat Cell Biol.* 2017;19(8):915-27.

44. Kerbel RS. Tumor angiogenesis: past, present and the near future. *Carcinogenesis.* 2000;21(3):505-15.

45. Kerbel RS. Tumor angiogenesis. *N Engl J Med.* 2008;358(19):2039-49.

46. Saharinen P, Eklund L, Pulkki K, Bono P, and Alitalo K. VEGF and angiopoietin signaling in tumor angiogenesis and metastasis. *Trends Mol Med.* 2011;17(7):347-62.

47. Jain RK. Antiangiogenesis strategies revisited: from starving tumors to alleviating hypoxia. *Cancer Cell.* 2014;26(5):605-22.

48. Jang K, Kim M, Gilbert CA, Simpkins F, Ince TA, and Slingerland JM. VEGFA activates an epigenetic pathway upregulating ovarian cancer-initiating cells. *EMBO Mol Med.* 2017;9(3):304-18.

49. Herr D, Sallmann A, Bekes I, Konrad R, Holzheu I, Kreienberg R, et al. VEGF induces ascites in ovarian cancer patients via increasing peritoneal permeability by downregulation of Claudin 5. *Gynecol Oncol.* 2012;127(1):210-6.

50. Devy L, Blacher S, Grignet-Debrus C, Bajou K, Masson V, Gerard RD, et al. The pro- or antiangiogenic effect of plasminogen activator inhibitor 1 is dose dependent. *FASEB J.* 2002;16(2):147-54.

51. Stefansson S, Petitclerc E, Wong MK, McMahon GA, Brooks PC, and Lawrence DA. Inhibition of angiogenesis in vivo by plasminogen activator inhibitor-1. *J Biol Chem.* 2001;276(11):8135-41.

52. Stefansson S, and Lawrence DA. The serpin PAI-1 inhibits cell migration by blocking integrin alpha V beta 3 binding to vitronectin. *Nature.* 1996;383(6599):441-3.

53. Wu J, Strawn TL, Luo M, Wang L, Li R, Ren M, et al. Plasminogen activator inhibitor-1 inhibits angiogenic signaling by uncoupling vascular endothelial growth factor receptor-2-alphaVbeta3 integrin cross talk. *Arterioscler Thromb Vasc Biol.* 2015;35(1):111-20.

54. Vargesson N. Thalidomide-induced teratogenesis: history and mechanisms. *Birth Defects Res C Embryo Today.* 2015;105(2):140-56.

55. Cortez AJ, Tudrej P, Kujawa KA, and Lisowska KM. Advances in ovarian cancer therapy. *Cancer Chemother Pharmacol.* 2018;81(1):17-38.

56. Karst AM, and Drapkin R. Primary culture and immortalization of human fallopian tube secretory epithelial cells. *Nat Protoc.* 2012;7(9):1755-64.

57. Sen P, Lan Y, Li CY, Sidoli S, Donahue G, Dou Z, et al. Histone Acetyltransferase p300 Induces De Novo Super-Enhancers to Drive Cellular Senescence. *Mol Cell.* 2019;73(4):684-98 e8.

58. Cox J, and Mann M. MaxQuant enables high peptide identification rates, individualized p.p.b.-range mass accuracies and proteome-wide protein quantification. *Nat Biotechnol.* 2008;26(12):1367-72.

59. Doberstein K, Spivak R, Feng Y, Stuckelberger S, Mills GB, Devins KM, et al. Fallopian tube precursor lesions of serous ovarian carcinoma require L1CAM for dissemination and metastasis. *bioRxiv* 2018;270785.

60. Zhou Y, Zhou B, Pache L, Chang M, Khodabakhshi AH, Tanaseichuk O, et al. Metascape provides a biologist-oriented resource for the analysis of systems-level datasets. *Nat Commun.* 2019;10(1):1523.

61. Strub T, Ghiraldini FG, Carcamo S, Li M, Wroblewska A, Singh R, et al. SIRT6 haploinsufficiency induces BRAF(V600E) melanoma cell resistance to MAPK inhibitors via IGF signalling. *Nat Commun.* 2018;9(1):3440.

62. Bader DA, Hartig SM, Putluri V, Foley C, Hamilton MP, Smith EA, et al. Mitochondrial pyruvate import is a metabolic vulnerability in androgen receptor-driven prostate cancer. *Nat Metab.* 2019;1(1):70-85.

63. Grote T, Siwak DR, Fritsche HA, Joy C, Mills GB, Simeone D, et al. Validation of reverse phase protein array for practical screening of potential biomarkers in serum and plasma: accurate detection of CA19-9 levels in pancreatic cancer. *Proteomics.* 2008;8(15):3051-60.

64. Kimbrel EA, Davis TN, Bradner JE, and Kung AL. In vivo pharmacodynamic imaging of proteasome inhibition. *Mol Imaging.* 2009;8(3):140-7.